POLITECNICO DI MILANO
School of Industrial and Information Engineering
Master of science in
Engineering Physics

Ultrafast Spectroscopy on Porphyrins Arrays for Light Harvesting

Supervisor: Prof. Giulio Cerullo
Co-Supervisor: Dr. Margherita Maiuri

Candidate:
Hana Irit Rabinowicz, matricola 877176

Academic Year 2018 - 2019

לאבא ואמא
וכמובן, לברי

Contents

Summary

In this research I explored the time-resolved spectroscopy of free base porphyrin. Specifically, I measured the dynamics of monomer, dimer and hexamer of free base porphyrin by an ultrafast spectroscopy. The dynamic of the three samples was gathered by a pump probe experiment while using a particular setup to generate a pump pulse in the range between 385 and 450 nm, and a probe pulse in the white light, covering the range from 420 to 740 nm. To be able to study the fast dynamics occurs in our sample we generated an ultra short pulse, shorter than 25 fs.

The global analysis result of the experimental data is as the following.
The first molecular transition is the vibration relaxation inside the S_2 energy level (smaller than 50 fs), we can see that the process is the longest for the monomer and the shortest for the hexamer while the dimer is in between. Though, the gap between all the three is almost equal. The second time constant is the internal conversion between the S_2 energy level to the S_{1-hot} energy level. As well as the first time constant, the second time constant is the longest in the monomer and the shortest in the hexamer.
On the contrary to the vibration relaxation dynamic, we can see that the internal conversion dynamic of the dimer and the hexamer samples behave in a similar form, both of them have a much shortest time decay (around 100 fs) respect to the monomer (around 326 fs). This fact point out the similarity of the molecular configuration of the dimer and the hexamer.
In addition, we obtained two additional processes, most probably they are indicate the vibration relaxation within S_1 energy level. The first process appears only in the dimer and hexamer samples with a time decay of few picoseconds. The second process occurs in all the samples and it equal to hundreds picoseconds or more. The last time decay is far from our measurement time range, thus we can not know the precise value of it.

Introduction

Ultrafast spectroscopy is an interdisciplinary powerful tool. The studying of the ultrafast dynamical processes is significant in chemical, solid-state, and biological materials. Research in ultrafast optics started roughly fifty years ago, and although this field is now tremendously active.
In this thesis I will focus on the pump probe spectroscopy, an ultrafast spectroscopy technique.
Pump probe spectroscopy is an advanced third-order non linear spectroscopic technique, allowing us to study the ultrafast dynamics of a system by measuring the optical polarization response.
This thesis is focused on the unique pump probe spectroscopy setup in the edge of the visible range, for the purpose of investigating the dynamics of the monomer, dimer and hexamer free base porphyrin molecules.
The porphyrin sample was synthesized in an innovative method in order to mimic the natural porphyrin that can be found in photosynthesis bacteria in nature[1].

In the first chapter I introduce the porphyrin molecule. I discuss its molecular structure, its molecular energy levels and its absorption spectrum.
In the second chapter I present the ultrashort pulse generation theory. I discuss the nonlinear optical generation in second and third order, and I elaborate about how it is used during the development of the experiment setup.
In the third chapter I discuss the pump probe spectroscopy. I explain the theory and the setup configuration that is used in order to investigate the molecular dynamics which appear in a very short time (~ 30 fs).
After the introduction of the theory that my experiment is based on, I present the setup which is based on the pump probe technique. The pump pulse I generated is between 385 and 450 nm, allowing to excite electronic transitions in the porphyrin samples. The probe pulse is a white light, covering the range from 420 to 740 nm.
Afterward, I present the uniqueness of the sample, its molecular structure and its absorption spectra. Furthermore, I introduce the global analysis method I used for the analysis of the experiment results.

In the last chapter, I present my experimental results. I discuss the ultrafast dynamic of the porphyrin free base samples. I elaborate on the differences and the similarities between the monomer, dimer and hexamer and I show the time constants of the samples.

Chapter 1

Introduction to Porphyrins

The porphyrin molecule belongs to the family of tetraphyrroles and is one of the most interesting molecule found in nature. Tetrapyrroles are a class of chemical compounds that contain four pyrrole with the formula C_4H_4NH.
Porphyrin has four nitrogen atoms facing the center, which can capture a metal ion and form a very stable organometallic complex. Porphyrins bind different metal ions, each of them gives to the porphyrin a specific biological functions. The natural porphyrins are fundamental for the development of vital functions of organisms.
The name "Porphyrin" derives from the Greek word porphyra meaning purple,but actually it can be found in variety of colors between purple to red, depending on the number of pyrrole units and the number of carbon atoms connecting the pyrrole units.[2]

Binding a prophyrin with iron for example lead to heme, a cofactor of the protein hemoglobin structure. Heme known as the component of the red pigment in blood cells.
Another important natural molecule is a porphyrin bound with coblat, forming Cobalamin that also known as B_{12} vitamin. B_{12} vitamin plays a key role in the normal functioning of the brain and nervous system and for the formation of blood. It is normally involved in the metabolism of every cell of the human body, especially affecting DNA synthesis and regulation, but also fatty acid metabolism and amino acid metabolism.
Chlorophylls are porphyrins with Magnesium. This structure is essential for photosynthesis process. The chlorophyll allows the first step of photosynthesis in plants, since they are response of the absorption of sun light, which is then transformed into chemical energy.[2]

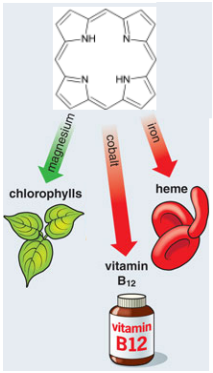

Figure 1.1: Binding of prophyrin with Magnesium, cobalt and Iron

1.1 Molecular Structure

A porphyrin is a group of ring structure macrocycle compound, composed of four modified pyrrole subunits (C_4H_5N), interconnected at their carbon atoms via methine bridges (=CH-)[3].

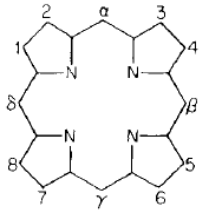

Figure 1.2: Molecular structure of Porphyrin

The most frequently substitution patterns of the prophyrin are β-octaalkylporphyrins, meso-tetraaryporphyrins and protoporphyrin IX. (figure 1.3)[4]

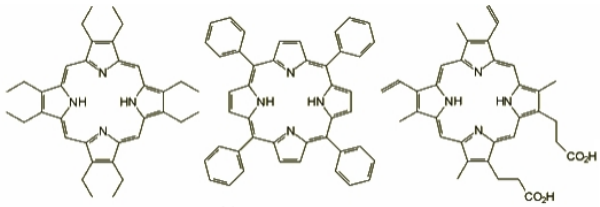

Figure 1.3: Favorite substitution patterns. Left: β-octaalkylporphyrins; Center: meso-tetraaryporphyrins; Right: protoporphyrin IX

The molecular structures of Chlorophyll, Hemoglobin and Cobalamin, discussed previously,are shown in figure 1.4

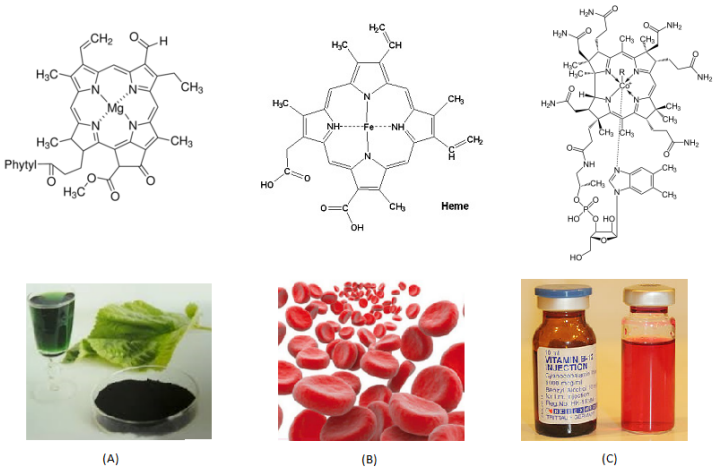

Figure 1.4: Molecular structure of (A) Chlorophyll (B) Hemoglobin (C) Cobalamin (vitamin B12)

1.2 Molecular Energy Levels

In 1960, Martin Gouterman proposed a "four-orbital" model to explain the absorption spectra of the porphyrins (figures 1.5 and 1.6). According to this theory, the absorption bands of the porphyrin arise from transition between the two highest occupied π orbitals (HOMOs) and the two lowest unoccupied π^* orbitals (LUMO). The HOMOs were calculated to be an a_{1u} and an a_{2u} orbital, while the LUMOs were calculated to be a degenerate set of e_g orbitals. The transitions between these orbitals gives two excited states. The higher energy state has greater oscillator strength, giving rise to an intense peak in the blue wavelength region of the visible spectrum (Soret band). The lower energy state has less oscillator strength and it gives rise to a range of frequencies contained in the visible region of the electromagnetic spectrum (Q-bands). Therefore, the electronic absorption spectrum of a porphyrin consist of two regions. The first region covers the transitions from the ground state to the first excited state in the range of 500-750 nm (the Q bands). The second region corresponds to the transition from the ground state to the second excited state which takes place in the range around 400 nm (the Soret or B band)[5][6][7][8].

We can describe the molecular energy landscape of a porphyrin by using the Jablonski diagram. The Jablonski diagram is a powerful tool for visualizing the possible transitions that can occur after a molecule has been photo excited. The diagram arranged with energy on a vertical axis, used to describe all the possible de-activation relaxation pathways upon the absorption of a photon by a molecule.(figure 1.7)[9]. S_1 and S_2 are used to describe the excited states imme-

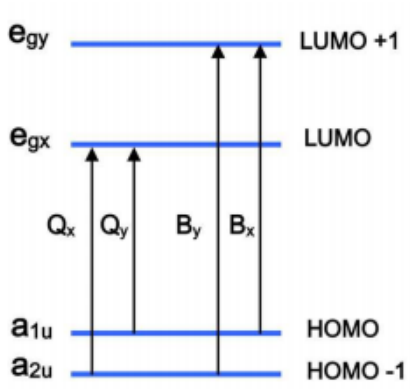

Figure 1.5: Energy levels of the four Goutermen orbials

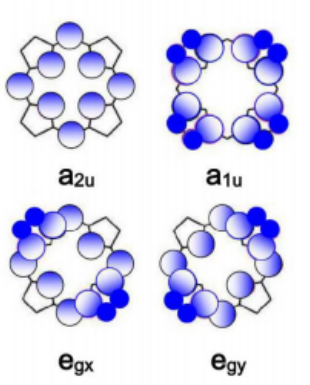

Figure 1.6: Four Goutermen orbials in porphyrin. **bottom row:***Porphyrin LUMOs* **top row:***Porphyrin HOMOs*

diately superior to the ground state. T is used to describe the triplet state.

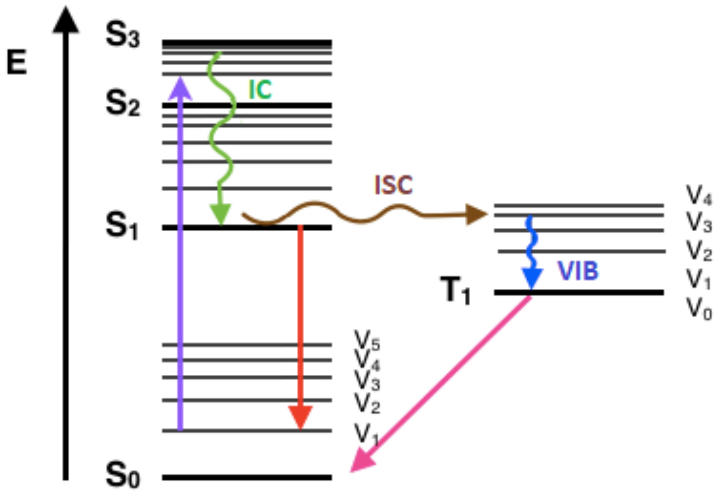

Figure 1.7: Jablonski diagram. Absorption, internal conversion (IC), intersystem crossing (ISC), vibrational relaxation (VIB), phosphorescence,fluoresence

I will mention six of the transition processes that can occur in the molecule. The first transition is the **absorption**. This is indicated by a straight arrow pointing up. Absorption is the method by which an electron is excited from a lower energy level to a higher energy level.
Once an electron is excited, there are a several ways by which the energy may be dissipated. The first is through **vibrational relaxation**, a non-radiative process. This is indicated on the Jablonski diagram as a curved arrow between vibrational

levels. Vibrational relaxation is where the energy deposited by the photon is given away to vibrational modes as kinetic energy. This kinetic energy may stay within the same molecule, or it may be transferred to other molecules around the excited molecule, largely depending on the phase of the probed sample. The average time scale of the vibrational relaxation is $10 - 10^4 fs$.
However, if vibrational energy levels strongly overlap with other electronic energy levels, a possibility exists that the excited electron can transition from a vibration level in one electronic state to another vibration level in a lower electronic state. This process is called **internal conversion** and mechanistically it identical to vibrational relaxation. It is also indicated as a curved line on a Jablonski diagram, between two vibrational levels in different electronic states. The average time scale of the internal conversion is $10 - 10^4 fs$.

All the processes described so far involve spin conservation, however it is possible to have relaxation where the electron changes spin multiplicity from an excited singlet state to an excited triplet state. This transition is called **intersystem crossing**. It is indicated by a horizontal, curved arrow from one column to another. The average time scale of the intersystem crossing is $10^7 - 10^{12} fs$. Intersystem crossing leads to several interesting routes back to the ground electronic state. One direct transition is **phosphorescence**, where a radiative transition from an excited triplet state to a singlet ground state occurs. Another possibility is **fluorescence**, the transition between the first excited electron state and the ground state.This is a slow process on the order of $10^6 - 10^8 fs$.

The relaxation time in the free base porphyrin molecule, according to previous researches are as the followings: less than 100 fs for intramolecular vibrational relaxation (VIB), 100-170 fs for internal conversion (IC) from S_2 to S_{1-hot}, between 10-20 ps for transition between S_{1-hot} to S_{1-cold}. Decay of the equilibrated S_{1-cold} population occurs on the nanosecond time scale by intersystem crossing to the triplet state T_1 (figure 1.8) [10][11][12][13][14].

1.3 Absorption Spectrum

The absorption spectrum of the porphyrin, according to previous researches is as the following [15][16]. The soret or B band has a single peak at 419 nm. The Q band splits because of the lower symmetry of the porphyrin into two components of unequal energy, Q_x and Q_y. We can define the Q band as a four satellite bands I-IV that observed at different wavelength which are as follows. Band I (Q_x) is located between 615-650 nm. Band II (Q_x) is found between 575-600 nm. Band III (Q_y) is observed between 525-560 nm and band IV (Q_y) is located between

Free Base Porphyrin- energy relaxation dynamic	
VIB in S2	<100 fs
IC s2 to hot s1	100-170 fs
VIB S1 hot to cold	10-20 ps
ISC S1 to T	ns

Figure 1.8: Relaxation time constant according to previous studies

500-530 nm. Based on the relative intensities of these four bands the spectra are classified into four types. Natural porphyrins with different substituents fall under these four types and can be easily identified.

the four Q-band spectrum is related to the degenerate in the D_{2h} symmetry of the free-base porphyrin. In contrast, combination of a porphyrin with a metal (metalloporphyrnis) are degenerate in the D_{4h} symmetry. Thus, it absorption spectrum included two Q-band spectrum[17]. The highest occupied π molecular orbitals (a_{1u} a_{2u} HOMOs) are very close in the energy to each other whereas the lowest unoccupied mulecolar orbitals (e_{gy} e_{gx} LUMOs) are double degenerate [18][19].

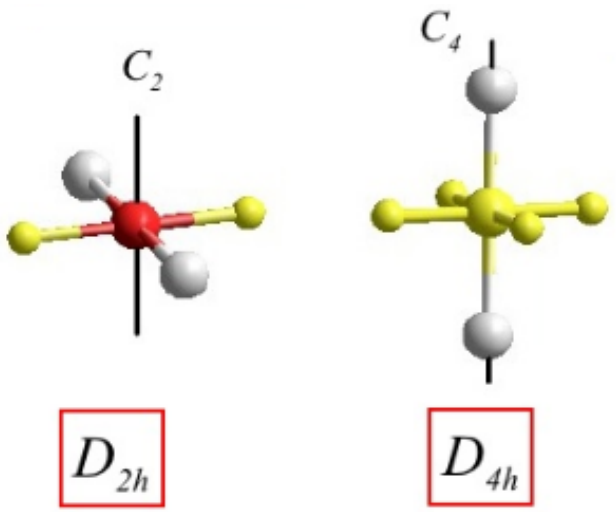

Figure 1.9: Point groups. **Left:** D_{2h} *and* **RIGHT:** D_{4h}

The first type is the **Etio-type spectra**. In this case the intensities of the four bands is in the sequences $IV > III > II > I$.

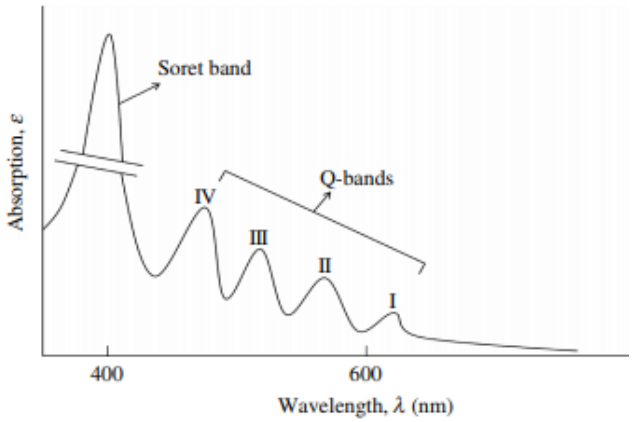

Figure 1.10: Typical free base Porphyrin absorption spectrum (etio- type)

The second type is the **Rhodo-type spectra** in which the intensities of the four bands is in the sequences $III > IV > II > I$.
Oxorhodo-type spectra is the third type, which the intensities of the four bands is in the sequences $III > II > IV > I$.
The fourth is **Phyllo-type spectra**, in which the intensities of the four bands is in the sequences $IV > II > III > I$

As a result of the different energy levels of the differenet binding molecules of the prophyrin, there are differences in the absorption spectrum of the group members of the porphyrins molecules [20].

For example, Chlorophyll is a green pigment found in chloroplasts of algae and plants. Chlorophyll absorbs light most strongly in the blue range of the electromagnetic spectrum, followed by the red range. Conversely, it has a poor absorption of green and near-green portions of the spectrum, hence the chlorophyll-containing tissues is green. There are two main absorption bands, the first one is on the red and the second one is on the blue. Two maxima between 600 nm and 700 nm correspond to absorption peaks of chlorophyll A and chlorophyll B.(figure 1.11)

Another example is the Hemoglobin absorption spectrum. The absorption peaks of the hemoglobin are at 579 nm and at 540 nm. (figure 1.12)
Finally, we can see the Cobalamin maxima absorption at 550 nm (figure 1.13).
As we can see, the absorption spectra changes according to the different metal the porphyrin is binding to.

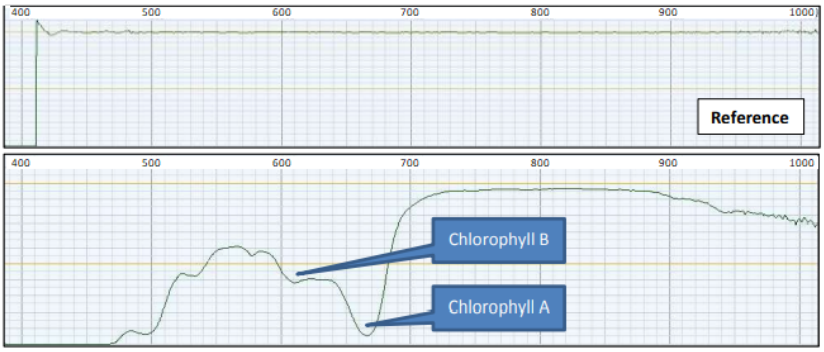

Figure 1.11: absorption (transmission) spectrum of chlorophyll solution in 95% ethanol [nm scale]

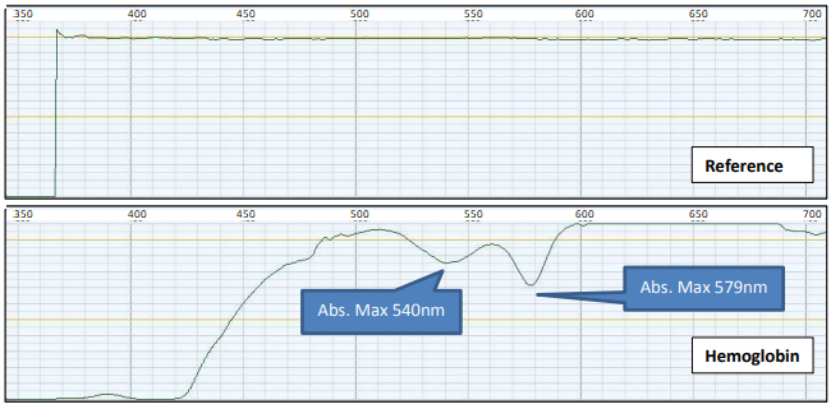

Figure 1.12: Hemoglobin absorption (transmission) spectrum [nm scale]

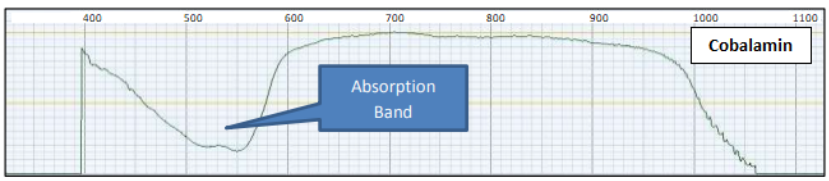

Figure 1.13: Cobalamin absorption (transmission) spectrum [nm scale]

Chapter 2

Ultrashort Pulse Generation

In the following chapter I will introduce and describe the theory of generation ultrashort pulse [21][22]. I will briefly present a review of Maxwell's equations, which describe the electromagnetic radiation.
Later, I will consider electromagnetic wave propagation in non-linear optics condition, in dispersive and non-dispersive medium.
All this theoretical background will lead to the demonstration of the collinear and noncolinear Optical Parameter Amplifier (OPA and NOPA) [23] [24].
Further, I will discuss the method to produce a White Light Generation (WLG).
Moreover, I will describe the method of pulse compensation after it propagate through a dispersive media.
Finally, I will describe the Frequency Resolved Optical Gating (FROG), a technique that provide a characterization of an ultraboardband pulses[25].

2.1 Pulse propagation

In order to describe the propagation of pulses in a medium, we need to start from Maxwell's equations:

$$\begin{cases} div\bar{D} = \rho \\ div\bar{B} = 0 \\ rot\bar{E} = -\frac{\partial B}{\partial t} \\ rot\bar{B} = \mu \cdot (\bar{J} + \frac{\partial D}{\partial t}) \end{cases} \tag{2.1}$$

where,

$$\begin{cases} \bar{D} = \epsilon_0 \bar{E} + \bar{P} \\ \bar{B} = \mu_0 \bar{H} + \bar{M} \end{cases}$$

For simplicity we can assume negligible magnetism $\bar{M} = 0$, no free charge

$\bar{\rho} = 0$ and no free current $\bar{J} = 0$.

From the Maxwell equations we obtain

$$\nabla^2 \bar{E} - \frac{1}{c_0^2}\frac{\partial^2 E}{\partial t^2} = \mu_0 \frac{\partial^2 P}{\partial t^2} \tag{2.2}$$

where $\epsilon_0 \mu_0 = \frac{1}{{c_0}^2}$

In our study, we assume:

1. Plane wave $E(x, y, z, t) \Rightarrow E(z, t)$
2. Electromagnetic wave are transverse $\bar{E} \perp \bar{B}$
3. Linear polarization

Therefore, we can rewrite the equation 2.2 as the following

$$\frac{\partial^2 E}{\partial^2 z} - \frac{1}{c_0^2}\frac{\partial^2 E}{\partial t^2} = \mu_0 \frac{\partial^2 P}{\partial t^2} \tag{2.3}$$

The polarization of the medium ,P, contain linear and non-linear parts

$$P(z, t) = P_L(z, t) + P_{NL}(z, t)$$

Hence, we will handle with the solution of 2.3 for the linear and non-linear cases separately. Of course, there is also a solution of pulse propagation in vacuum, $P = 0$. In this case the solution of the pulse equation 2.3 is

$$E(z, t) = A(z, t)cos(\omega_0 t - k_0 z + \phi(z, t)) \tag{2.4}$$

Where $A(z, t)$ represent the envelope wave, and $cos(\omega_0 t - k_0 z + \phi(z, t))$ represent the carrier wave. We can write the solution in an equivalent way

$$E(z, t) = A(z, t)e^{(\omega_0 t - k_0 z)} \tag{2.5}$$

2.2 Linear Optics

The linear part of the polarization P_L is defined as

$$P_L(z, t) = P_L(z, t)e^{i(\omega_0 t - k_0 z)} \tag{2.6}$$

By plugging the polarization term in the pulse equation 2.3, while approximating a slow varying of the envelope part of the function we get

$$-k_0^2\tilde{A} - 2ik_0\frac{\partial\tilde{A}}{\partial Z} + \frac{\tilde{\omega}}{c_0^2}\tilde{A} = -\mu_0\omega^2\tilde{P_L} \tag{2.7}$$

The polarization is defines as:

$$\tilde{P_L}(\omega) = \epsilon_0\chi^{(1)}\tilde{E}(\omega) = \epsilon_0[n^2(\omega) - 1]\tilde{A}(\omega) \tag{2.8}$$

Therefore, we can rewrite the pulse equation 2.3

$$-2ik_0\frac{\partial\tilde{A}}{\partial Z} + [k^2(\omega) - k_0^2(\omega_0)]\tilde{A} = 0 \tag{2.9}$$

Where $k^2(\omega) = \frac{\omega^2}{c^2(\omega)}$
Under the assumption of very small FWHM, the approximation that can be taken is $k(\omega) + k_0(\omega_0) = 2k_0(\omega_0)$. Thus, the term $k^2(\omega) - k_0^2(\omega_0)$ can be expanded as a Taylor expansion of the wave vector k around the frequency $\omega - \omega_0$.

$$k^2(\omega) - k_0^2(\omega_0) = 2k_0(\omega_0)[\frac{\partial k}{\partial\omega}|_{\omega_0}(\omega - \omega_0) + \frac{1}{2}\frac{\partial^2 k}{\partial\omega^2}|_{\omega_0}(\omega - \omega_0)^2...] \tag{2.10}$$

We will only consider the three first terms of the Taylor series. Plug this term back in equation 2.9, and convert back to time domain by Fourier Transform, one can get:

$$\frac{\partial A}{\partial Z} + \frac{\partial k}{\partial\omega}|_{\omega_0}\frac{\partial A}{\partial t} - i\frac{1}{2}\frac{\partial^2 k}{\partial\omega^2}|_{\omega_0}\frac{\partial^2 A}{\partial t^2} = 0 \tag{2.11}$$

The pulse is propagating at group velocity v_g, defined by the velocity propagation of the pulse's envelope

$$\frac{1}{v_g} = \frac{\partial k}{\partial\omega}|_{\omega=\omega_0} \tag{2.12}$$

The group velocity dispersion (GVD) is defined as

$$GVD = \frac{\partial^2 k}{\partial\omega^2}|_{\omega_0} \tag{2.13}$$

For better understanding the influence of the medium on the pulse propagation, we rewrite the parabolic equation in the time and frequency domain. By shifting the perspective to the wave front through a change of variable the equation simplifies to

$$\frac{\partial A}{\partial Z} - \frac{i}{2}K''_{\omega_0}\frac{\partial^2 A}{\partial t^2} = 0 \tag{2.14}$$

$$\frac{\partial \tilde{A}}{\partial Z} = -\frac{i}{2} K''_{\omega_0} \tilde{A} \omega^2 \tag{2.15}$$

When $GVD = 0$ the medium is **non-dispersive**. This means that at any point in space, the temporal shape of the pulse is the same $A(z,t) = A(t)$.

In the case of $GVD \neq 0$ the medium is **dispersive**. The different components of the pulse will have different phase velocities. In the case of positive GVD, the lower frequencies travel faster than higher frequencies. As a result, the wave packet spreads out with the longer wavelengths moving faster and the shorter wavelengths lagging behind. Moreover, The shorter the pulse is, the stronger the dispersion.

Now, consider a block of dispersive medium with length L on the z direction. Suppose that the pulse envelope is located in $z = 0$,the solution of equation 2.15 is

$$\tilde{A}_{(0,\omega)} = \tilde{A}_{(0)} e^{-\frac{i}{2} D_2 \omega^2} \tag{2.16}$$

where $D_2 = GDD = \frac{\partial^2 k}{\partial \omega^2}|_{\omega=\omega_0} L$ is the second order of dispersion, called the group delay dispersion (GDD). Notice that GDD depends on the medium of propagation as well on the length of the dispersive material it passes through.

The result of propagation of the pulse in a distance L is:

$$\tilde{A}_{(L,\omega)} = \sqrt{2\pi} \tau_p \tilde{A}_{(0)} e^{\frac{-\omega^2 \tau_p^2}{2}(1+\frac{iD_2}{\tau_p^2})} \tag{2.17}$$

In the time domain we obtain

$$A_{(L,t)} = \frac{A_0 \tau_p}{\sqrt{\tau_p^2 + iD_2}} e^{\frac{-t^2}{2\tau_{out}^2}} e^{i\varphi(t)} \tag{2.18}$$

Where I defined the time factor τ_{out} as:

$$\tau_{out} = \tau_p \sqrt{1 + (\frac{D_2}{\tau_p^2})^2} \tag{2.19}$$

We got that the output duration of the pulse, τ_{out}, is bigger than the input duration τ_p since it is multiplied by a term bigger than one.
If $D_2 << \tau_p^2$, we get $\tau_{out} \approx \tau_p$. The dispersion is very small so the pulse does not change.
if τ_p is small, we get $\tau_{out} \approx \frac{D_2}{\tau_p}$. The broadening is almost linear with respect to propagation distance. Taking that into account, the electric field can be written

as

$$E(t) = |A(t)|e^{i[\omega_0 t + \phi(t) - k_0 z]} \tag{2.20}$$

The instantaneous frequency is

$$\omega(t) = \frac{d}{dt}[[\omega_0 t + \phi(t)] = \omega_0 + \frac{D_2 t}{2(\tau_p^4 + D_2^2)} \tag{2.21}$$

We notice that the instantaneous frequency is not a constant. It can increase or decrease on time, depending on the sign of the group delay dispersion D_2. In the case of $D_2 > 0$ we are dealing with **positive chirp** (up-chirp)- the frequency is increases during the pulse propagation. The different wavelengths have a different speed. The lower frequencies have higher speed with respect to the higher ones, which get delayed. In the opposite case, $D_2 < 0$ we are having a **negative chirp** (down-chirp)- the frequency decreases during the time. The pulse will start with high frequency and will finish with a low one, the highest frequency will be the slowest and the lower frequency will be the faster. In the both cases, if the pulse is short enough all the frequencies will arrive together.
As will be better explained in following chapters, pulses duration is related to temporal resolution in experiments. With this in mind, it is fundamental to investigate the temporal broadening of a pulse due to these effects.

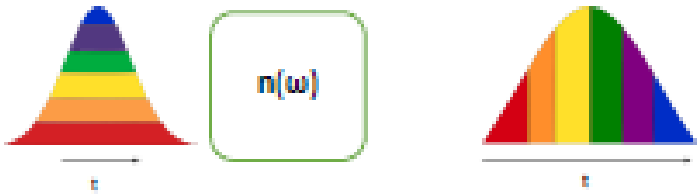

Figure 2.1: A short pulse is enter to a dispersive medium. As a result, the output pulse that obtain is longer

2.3 Non Linear Optics

The total polarization can be expressed as a linear and a non linear terms:

$$P(z,t) = P_L(z,t) + P_{NL}(z,t)$$

From equation 2.8:

$$P = \epsilon_0[\chi^{(1)}E + \chi^{(2)}E^2...] \tag{2.22}$$

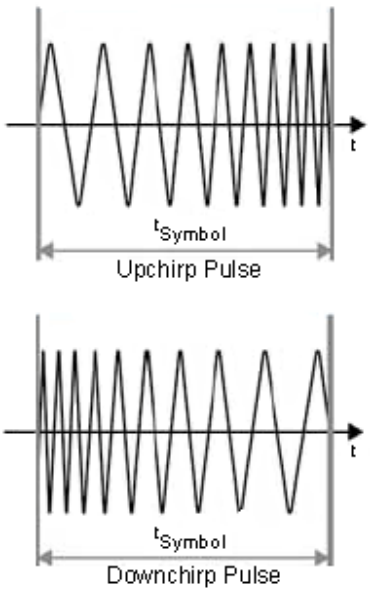

Figure 2.2: up chirp- the frequency of the pulse is increases. down chirp- the frequency of the pulse is decreases

The non linear polarization can be written as

$$\mathbf{P}_{NL}(z,t) = P_{NL}e^{i(\omega_0 t - k_P z)}$$

The electric field is:

$$\mathbf{E}(z,t) = A(z,t)e^{i(\omega_0 t - k_0 z)}$$

The pulse propagation can be described by the following equation

$$\frac{\partial A}{\partial Z} + \frac{1}{v_{g_0}}|_{\omega_0}\frac{\partial A}{\partial t} - i\frac{1}{2}\frac{\partial^2 k}{\partial \omega^2}|_{\omega_0}\frac{\partial^2 A}{\partial t^2} = i\mu P_{NL}\frac{\omega_0 c_0}{n_0}e^{-i\Delta k z} \tag{2.23}$$

where $\Delta k = k_p - k_0$ and $\frac{\omega_0}{k_0} = c = \frac{c_0}{n_0}$

2.3.1 Second Order Nonlinear Optics

Consider a case of two-wave mixing propagating in a non-linear medium. The field equation is

$$\mathbf{E}(z,t) = A_1 e^{i\omega_1 t} + A_1^* e^{-i\omega_1 t} + A_2 e^{i\omega_2 t} + A_2^* e^{-i\omega_2 t} \tag{2.24}$$

The non-linear polarization, as defined in 2.22, is $P = \epsilon_0 \chi^{(2)} E^2$.
In the case of two-wave mixing, we can plug in the field equation 2.24 and the non

linear polarization can be written as:

$$P_{NL} = \epsilon_0 \chi^{(2)}[E(z,t)] = \epsilon_0 \chi^{(2)}[(i) + (ii) + (iii) + (iv)]$$

Where
(i) $A_1^2 e^{2i\omega_1 t} + A_1^{*^2} e^{-2i\omega_1 t} + A_2^2 e^{2i\omega_2 t} + A_2^{*^2} e^{-2i\omega_2 t}$
(ii) $2A_1 A_1^* + 2A_2 A_2^*$
(iii) $2A_1 A_2 e^{i(\omega_1+\omega_2)t} + 2A_1^* A_2^* e^{-i(\omega_1+\omega_2)t}$
(iv) $2A_2 A_1^* e^{i(\omega_2-\omega_1)t} + 2A_1 A_2^* e^{-i(\omega_2-\omega_1)t}$

The first element is the **Second Harmonic Generation (SHG)**. This element include term with $2\omega_1$ or $2\omega_2$ phase.
The second element describe terms with zero phase.
The third element is the **Sum Frequency Generation (SFG)** and include terms with $\omega_1 + \omega_2$ phase.
The forth element is the **Difference Frequency Generation (DFG)** and include terms with $\omega_2 - \omega_1$ phase.

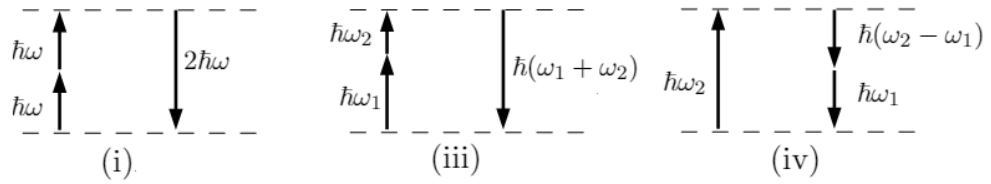

Figure 2.3: (i) Second Harmonic Generation (SHG); (iii) Sum Frequency Generation (SFG) (iv) Difference Frequency Generation (DFG)

We can expand this study to a three monochromatic waves mixing, entering into a second order material. From equation 2.23 we can obtain three coupled equations

$$\begin{cases} \frac{\partial A_1}{\partial Z} = -i\gamma_1 A_3 A2^* e^{-i\Delta K Z} \\ \frac{\partial A_2}{\partial Z} = -i\gamma_2 A_3 A1^* e^{-i\Delta K Z} \\ \frac{\partial A_3}{\partial Z} = -i\gamma_3 A_1 A2^* e^{-i\Delta K Z} \end{cases} \tag{2.25}$$

Where $\gamma_i = \frac{\omega_i \chi 6(2)}{4 n_i c_0}$ and $\Delta k = k_3 - k_1 - k_2$

2.4 Optical Parametric Amplification (OPA)

The Optical Parametric Amplification (OPA), is a process of the second order nonlinear optics which exploits the DFG. It allows the amplification of a week signal at a specific frequency (ω_s) by using a strong pump wave at (ω_p), such that the signal at (ω_s) will be amplified when (ω_p) and (ω_s) are incident into a non centro-symmetric crystal which exploits second order non linear susceptibility. At the output, the signal wave is amplified and a new idler wave at ω_i is generated (figure 2.4).

$\omega_i + \omega_s = \omega_p$

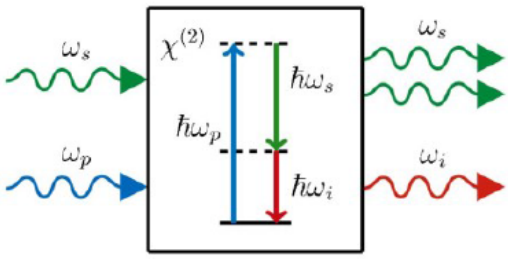

Figure 2.4: Optical Parametric Amplification (OPA) scheme.

It is worth emphasizing that the gain in an OPA occurs only for a narrow temporal window during which the pump and signal pulses are overlapping. The extent of this window is determined by the pump duration and the pump-signal temporal walk-off and is limited to at most a few hundred femtoseconds under typical conditions.

Using the coupling equations 2.25, and considering a non depletion approximation $A_3(z) = A_3(0) \equiv A_{30}$, the Parametric Gain that obtain is

$$G(z) = \frac{I_2(z)}{I_2(0)} = \begin{cases} \frac{1}{4} exp(2\Gamma z) & \text{if } \Delta k = 0 \\ \frac{\Gamma^2}{4g^2} exp(2gz) & \text{if } \Delta k \neq 0 \end{cases} \tag{2.26}$$

Where $\Gamma^2 = \frac{\omega_1 \omega_2 \chi^{(2)^2}}{16 n_1 n_2} |A_{30}|^2$ and $g = \sqrt{\Gamma^2 - (\frac{\Delta k}{2})^2}$

Firstly, we discuss about the phase matching case. We can observe that the gain is exponentially increasing with the wave propagation in the Z direction. Moreover, for having a high gain we would like to increase $\Gamma \propto |A_{30}|$, the meaning is to use an ultrashort pulse.

In the case of phase mismatching, the gain is exponentially dependent on g. When the Δk increases, the g decreases and the gain become lower.

In order to satisfy the phase match condition, the refractive index needs to follow

the upcoming condition

$$\Delta k = k_3 - k_1 - k_2 = 0$$

$$\omega_3[n(\omega_3) - n(\omega_2)] = \omega_1[n(\omega_1) - n(\omega_2)] \tag{2.27}$$

Assuming $\omega_2 > \omega_1$. In bulk isotropic material in the normal dispersion region we get $n_3 > n_2 > n_1$ so the left side of the equation is giving a positive value, whereas the right one is negative. Therefore, one can think that the phase matching condition can not be obtained. To solve the problem we have to use birefringent crystal. There are two types of birefringence based solution we can use:

Type I: The pump beam is polarized along the extraordinary direction while both the idler and signal are polarized in the ordinary direction, perpendicular to the pump beam (on the extraordinary).

$$\omega_3 n_e(\omega_3, \theta_m) = \omega_1 n_0(\omega_1) + \omega_2 n_0(\omega_2)$$

Type II: The pump beam is polarized along the extraordinary direction. The signal or the idler beam is polarized in the extraordinary direction while the other is polarized perpendicular.

$$\text{or} \begin{cases} \omega_3 n_e(\omega_3, \theta_m) = \omega_1 n_0(\omega_1) + \omega_2 n_e(\omega_2, \theta_m) \\ \omega_3 n_e(\omega_3, \theta_m) = \omega_1 n_e(\omega_1, \theta_m) + \omega_2 n_e(\omega_2) \end{cases}$$

The phase matching condition can be achieved by adjusting the angle between the wave vector of the propagating beams and the optical axis of the nonlinear crystal.

In the case of three pulses propagating in a nonlinear crystal with different group velocities, we should achieve also a group velocities matching. For this we need to consider a range of frequencies $\Delta\omega$ that need to be amplified. For instance, let's take a range of signal's frequencies $\omega_2 = \bar{\omega_2} + \Delta\omega$ hence $\omega_1 = \bar{\omega_1} - \Delta\omega$. We can find the condition of phase matching as a function of the group velocities of the Idler and the Signal

$$\Delta k = \Delta\omega[\frac{1}{v_{g2}} - \frac{1}{v_{g1}}] \equiv \Delta\omega\delta_{21} \tag{2.28}$$

The easiest way to obtain phase matching condition (i.e. $\delta = 0$) is when idler beam and signal beam have the same frequency:

$$\delta_{21} = \frac{1}{v_{g2}} - \frac{1}{v_{g1}} = 0 \Rightarrow v_{g2} = v_{g1}$$
$$\omega_1 = \omega_2$$

In this case we have a type I phase matching and we can achieve this in a collinear geometry. We will describe below how to obtain a phase matching condition also with a non collinear geometry.

2.5 Non Collinear Optical Parameter Amplifier (NOPA)

In the noncolinear configuration, there is an additional degree of freedom. The phase matching is a vector condition, not a scalar as before. The relation between the wave vectors are

Parallel:	$K_3 cos(\alpha) = K_2 + K_1 cos(\Omega)$
Perpendicular:	$K_3 sin(\alpha) = K_1 sin(\Omega)$

As sowing in figure 2.5

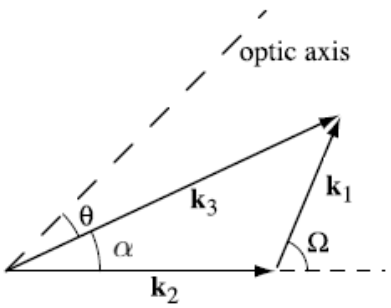

Figure 2.5: NOPA wave vectors

In order to satisfy the phase matching condition we should implement a specific angle for having $\Delta K_{par} = 0$ and $\Delta K_{per} = 0$. In consequence, the condition for a phase matching is

$$v_{g2} = v_{g1} cos(\Omega) \tag{2.29}$$

The collinear and the noncolinear cases can be seen in figure 2.6. In figure 2.6(a) we have a collinear case with $v_{g1} > v_{g2}$ and unequal phase. In the case of 2.6(b), the propagation is dictated by equation 2.29. Therefore, even the green is propagating faster, they both eventually remain in the same phase. With the

noncolinear method we can broaden the bandwidth while choosing non degenerate frequencies $\omega_1 \neq \omega_2$.
On figure 2.7 one can see phase matching curves for a type I BBO crystal, pumped at $0.4\mu m$, as a function of the pump-signal angle for different values of pump- signal angle α. When $\alpha = 0$ we have a case of collinear OPA. We can observe the strong dependency of the signal wavelength in the phase matching angle, which means that we will get a narrow signal frequency range for specific crystal orientation. Changing the configuration to be noncollinear OPA, increasing the pump-signal angle α is leading to a wider signal frequency range for a fixed crystal orientation. As can be seen in figure 2.7, the optimum noncollinear configuration is obtained in $\alpha = 3.7^0$, where the phase matching angle is constant for wider signal wavelengths.

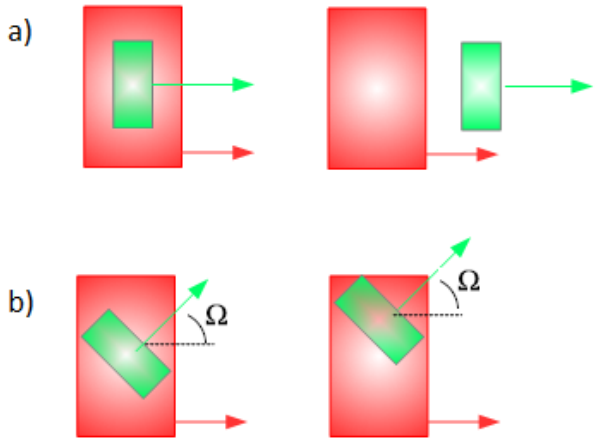

Figure 2.6: (a)Collinear propagation with inequal velocities and phases (b) Noncollinear propagation with unequal velocities, but equal phase

2.6 OPA and NOPA

2.6.1 OPA design

As mentioned before, a general OPA technique contain an interaction between a weak signal beam with a strong pump beam. A femtosecond OPAs are in general pumped by amplified Ti:sapphire lasers. The pump can be at the fundamental ($0.8\mu m$) or at the second harmonic ($0.4\mu m$) of the laser.
As can be seen in figure 2.8, the OPA is generate an initial signal beam, the so called 'seed' beam. For the generation of the seed beam, one can use white light continuum generation (see section 2.7). After the generation of the seed beam, the seed combines with a pump beam in a nonlinear crystal in the parametric

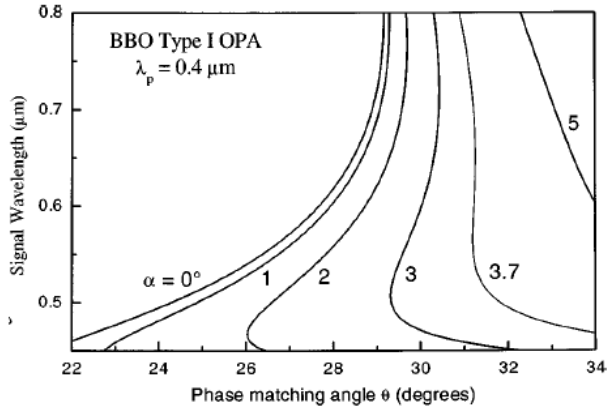

Figure 2.7: Phase-matching curves for a noncollinear type I BBO OPA pumped at $0.4\mu m$*, as a function of the pump-signal angle* α*.*

amplification stage. It is necessary to have a temporal overlap between the two beams. Afterward, the signal idler and the pump beams are separated from each other. In the case of broadband amplification, a pulse compressor is used to obtain transform-limited pulse duration (see section 2.8).

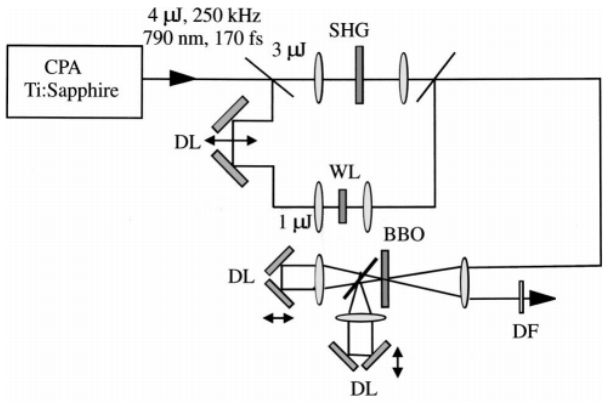

Figure 2.8: Scheme of visible OPA

2.6.2 NOPA design

In the visible, relatively long pump pulses ($\approx 100fs$) are used and the properties of noncollinear phase matching are exploited to achieve broadband amplification of the white-light seed. The amplified pulses are then compressed to sub-10 fs duration using suitable compression.

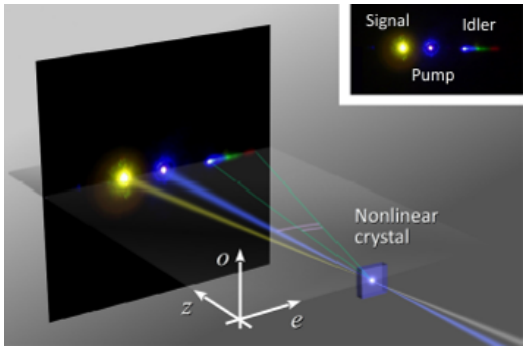

Figure 2.9: Non-collinear OPA configuration,exploiting the angle between the three beams.

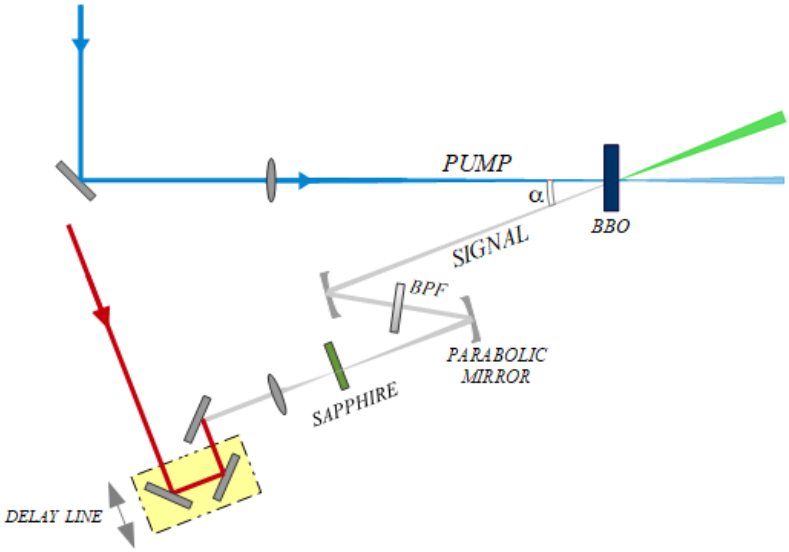

Figure 2.10: Non-collinear optical amplifier.

OPAs tunable in the near-IR are the most straightforward to operate. The main advantages is the high availability of pump energies and low pump- signal and pump-idler GVM values (Group Velocity Mismatch between the interacting pulses). The low GVM allows the use of long nonlinear crystal make it possible to obtain a high gain.

For designing a visible NOPA, a pump pulse we will use the following method.

Pumping with (second harmonic) SH of a Ti:sapphire laser around $0.4\mu m$, the signal can be tuned through most of the visible range, from around $0.45\mu m$ to degeneracy ($0.8\mu m$). Correspondingly, the idler tunes from $0.8\mu m$ to 2.5. this fills the gap in the tuning range for near-IR OPAs.

Visible NOPAs in general obtain lower energies than near-IR ones, because of the lower pump energy available from a frequency doubled pump. Furthermore the GVM is much larger in the visible range, which limits the use of long nonlinear crystals. This disadvantage is partially compensated for by the larger figures of merit for parametric interaction in the visible.

2.7 White Light Generation (WLG)

is a third order process. and occurs when an intense ultrashort pulse is focused inside a transparent material such as fused silica or sapphire. As a result of the interplay between **self-focusing** which is responsible for very high peak intensities, and **self phase modulation** which leads to the generation of the new frequencies, a large spectral broadening takes place. Under the correct conditions, the white light has an excellent spatial quality, with a circular gaussian beam and a very high pulse-to-pulse stability.

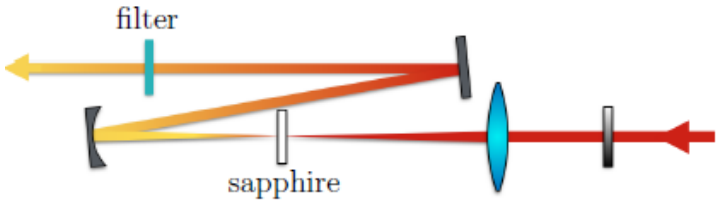

Figure 2.11: White Light Generation setup

$$P_{NL}(z,t) = \epsilon_0 \chi^{(3)} E^3(z,t)$$

In the third order, four wave mixing are involved (see figure 2.12). The degenerate frequencies in the case are as the following

$$\omega_1 = \omega_2 = \omega_3 = \omega$$
$$\omega_4 = \omega_1 + \omega_3 - \omega_2 = \omega$$

The non- linear Schrodinger equation is

$$\frac{\partial A}{\partial Z} - iGVD\frac{\partial^2 A}{\partial t^2} + i\gamma|A|^2 A = 0 \tag{2.30}$$

Where $\gamma \propto \chi^{(3)}$

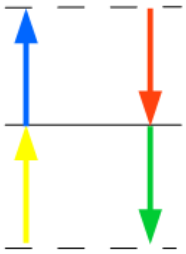

Figure 2.12: Fegenerate Four Wave Mixing

The second element in equation 2.30 represent the dispersion, while the third element represent the Self Phase Modulation (SPM).

2.7.1 Self- focusing

The Self-Focusing effect is a third order non-linear optical process induced by the change in refractive index of materials exposed to intense electromagnetic intensity. Starting from the polarization, and neglecting the second order non-linear term (which is different from zero only in centro-symmetric media):

$$P = \epsilon_0(\chi^{(1)} + \chi^{(3)}|A|^2)E \tag{2.31}$$

We define $\chi_{eff} = (\chi^{(1)} + \chi^{(3)}|A|^2)$. Given that $\chi_{eff} = n^2 - 1$ where n is the refractive index.

$$n^2 = \chi_{eff} + 1 = 1 + \chi^{(1)} + \chi^{(3)}|A|^2 = n_0^2 + \chi^{(3)}|A|^2 \tag{2.32}$$

By making a Taylor expansion, one obtains:

$$n = n_0\sqrt{1 + \frac{\chi^{(3)}|A|^2}{n_0^2}} \approx n_0 + \frac{\chi^{(3)}}{2n_0}|A|^2 = n_0 + n_2|A|^2 \tag{2.33}$$

The refractive index has a dependence on the intensity of the wave. If the mode has a gaussian spatial profile, the center of the beam will experience an higher (or lower) refractive index, and the medium will act as a focusing (or defocusing) lens. If a medium has a positive value of $\chi^{(3)}$, it is self-focusing. if $\chi^{(3)}$ is negative the medium is self-defocusing.

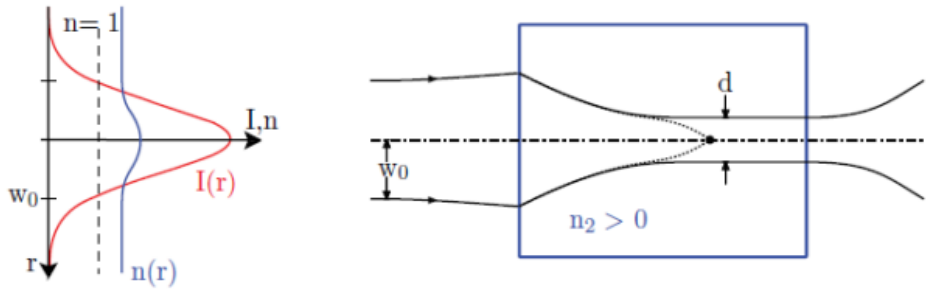

Figure 2.13: The Self-Focusing effect for a bell shaped beam intensity. In the crystal occurs an effect that similar to a wave guide.

2.7.2 Self Phase Modulation (SPM)

Consider a material with negligible group velocity dispersion $GVD \approx 0$. The solution of equation 2.30 will be

$$A(z,t) = A(0,t)e^{-\gamma|A(0,t)^2 z|} \tag{2.34}$$

Assumed intensity is not dependent on Z.

$$E(z,t) = A(z,t)e^{i(\omega_0 t - k_0 z)} = A(0,t)e^{i\Phi(z,t)} \tag{2.35}$$

The instantaneous frequency can be obtained by the derivative of the phase term

$$\omega_i(t) = \frac{\partial \Phi}{\partial t} = \omega_0 - \gamma z \frac{\partial}{\partial t}|A(0,t)|^2 \tag{2.36}$$

The instantaneous frequency is modulated according to the time derivative of the intensity.
From the equation 2.36 one can notice that for a simple Gaussian shape of the pulse intensity, the derivative of the intensity profile is obtain two peak points- high and low. The two peaks are refer to the change of curvature. As can be seen, propagation broadens the spectrum symmetrically towards the blue and the red (figure 2.14).

2.8 Pulse Compression

During the propagation, the pulse affected by propagation through a dispersive media. The dispersion varys the pulse duration and the pulse quality and causes a certain chirp that must be compensated in order to achieve the best measure. Therefore, a pulse compressor is needed.

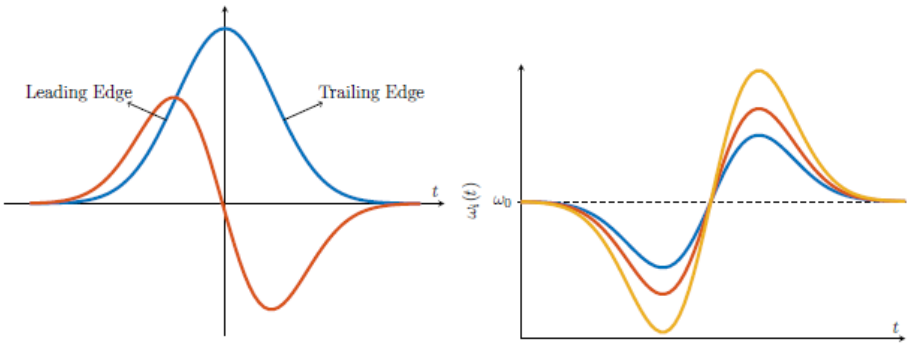

Figure 2.14: **LEFT:** *Squared absolute value of field amplitude, and its time derivative.* **RIGHT:** *Frequencies below ω_0 are generated by the leading edge, frequencies above by the trailing edge.*

Consider a pulse $E_{in}(\omega) = |E_{in}(\omega)|e^{-i\phi_{in}(\omega)}$ entering to a pulse compressor with transfer function of $T(\omega) = e^{-i\phi_{comp}(\omega)}$. The output that will be obtained is

$$\begin{aligned}\tilde{E}_{out}(\omega) =& |\tilde{E}_{in}(\omega)|e^{-i\phi_{in}(\omega)}T(\omega) \\ =& |\tilde{E}_{in}(\omega)|e^{-i[\phi_{in}(\omega)+\phi_{comp}(\omega)]}\end{aligned}$$

For achieving the maximum pulse quality, the pulse compressor should compensate the dispersion of the pulse. Therefore, the second and third orders of the total dispersion need to be equal to zero

$$D_{2out} = \frac{\partial^2\phi_{out}}{\partial\omega^2}|_{\omega_0}L = D_{2in} + D_{2comp} \equiv 0 \tag{2.37}$$

$$D_{3out} = \frac{\partial^3\phi_{out}}{\partial\omega^3}|_{\omega_0}L = D_{3in} + D_{3comp} \equiv 0 \tag{2.38}$$

We can rewrite the conditions

$$D_{2comp} = -D_{2in} \tag{2.39}$$

$$D_{3comp} = -D_{3in} \tag{2.40}$$

In the visible D_{2in} , $D_{3in} > o$ hence the the requirement of the compression dispersion is $D_{comp} < 0$.

There are few optical components suitable for pulse compression. For instance, grating pair, prism pair compressor and chirped mirrors.
Prism pair method for example, is an angular dispersion device that is commonly used. As can be seen in figure 2.16, the compressor is made by the configuration of two prisms.

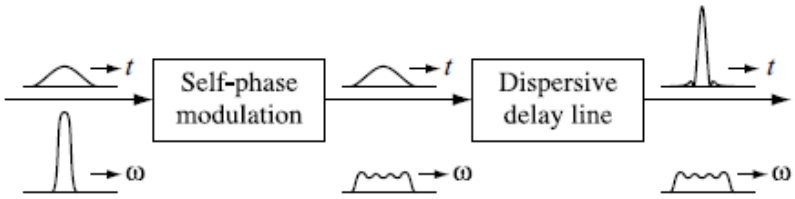

Figure 2.15: Block diagram view of optical pulse compression

The overall dispersion can be tuned by translating one of the prisms in a direction perpendicular to its base, which varies the material path length L_g without affecting the angular dispersion.
The advantageous of the prism pair is low loss, cheap and easy to tune the sign and the magnitude of the dispersion. The main limitation is relatively low angular dispersion, which increases the required prism spacing and restricts the magnitude of temporal dispersion that prism sequences can provide.

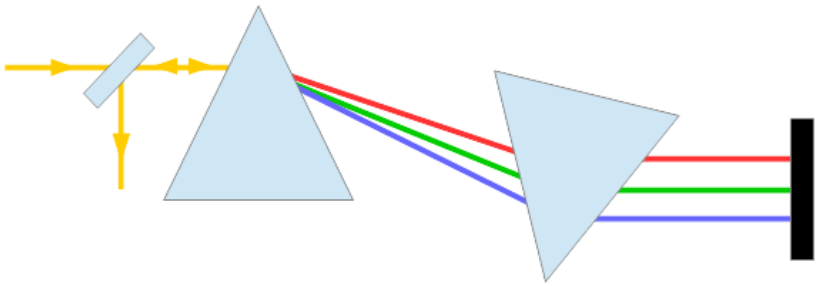

Figure 2.16: Prisms pair compressor

A chirped mirror design uses dielectric mirrors with variable thickness λ_B as can be seen in figure 2.17. The idea is that each optical frequency component should reflect mainly from that part of the mirror where λ_B matches the Bragg condition of diffraction. Therefore, different frequencies should be reflected after penetrating different layers, resulting in a frequency-dependent delay. This device is expected to provide negative dispersion, since longer wavelengths would experience larger delay. This would be useful for compensating for positive material dispersion.

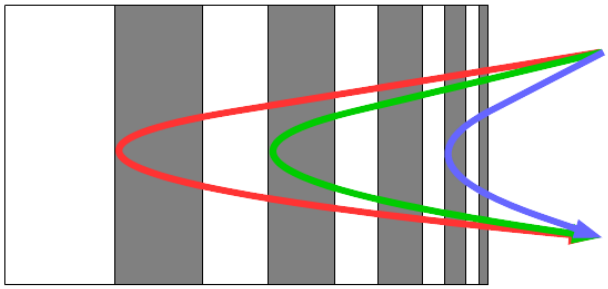

Figure 2.17: Chirped mirror designed to provide negative dispersion

Chapter 3

Ultrashort Spectroscopy

Ultrafast laser spectroscopy is a technique that uses ultrashort pulse lasers in order to study the dynamical processes in chemical, solid state and biological materials on extremely short time scales. [21][22][26].
A large number of different ultrafast spectroscopy schemes may be understood within the framework of the pump-probe approach as illustrated in figure 3.1. A short **pump** pulse first impinges upon the sample under investigation and excites it. This excitation induces a change in the material property P. In most cases we are interested in an optical property of the material.
We may write

$$P(t) \rightarrow P_0 + \Delta P(t - t_0) \tag{3.1}$$

Where $P_0 + \Delta P$ is the initial value of property P and the change in P induced by a pump pulse arriving at time t_0, respectively.
A second pulse, termed the **probe**, arrives at the sample with time delay T with respect to the pump pulse. The intensity of the probe pulse is kept small compared to that of the pump pulse. By detecting the probe pulse after the interaction with the sample, we can get information about ΔP at time $t - t_0 = T$. By performing a series of measurements in which delay T is varied, we monitor of the full time dependence of the material response function $\Delta P(T)$. In fact, this is a correlation function approach, adapted for spectroscopic purposes. By relating the measured material response function to a microscopic model of the physical processes under investigation, one attempts to gain insight into the dynamics of these processes.
In practice, the material property P that we investigate is the **polarization** of the sample. We will use the relation $E^{(3)}(T,t) \propto iP^{(3)}(T,t)$,where T is the delay of the probe pulse with respect to the pump, in order to study a sample. We would like to measure the third order field $E^{(3)}$ in order to find information about the third order polarization.

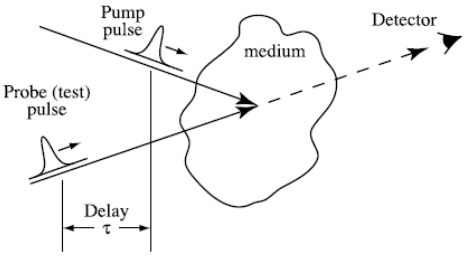

Figure 3.1: Pump Probe approach

3.1 Pump-Probe

In a pump-probe experiment two pulses are involved. The pump pulse is the first pulse, interacts with the sample creating a population inversion. The probe pulse, which impinges the sample at delay of T with respect to the pump, is the one that generates the third order polarization exactly the same direction as the probe pulse (figure 3.2).

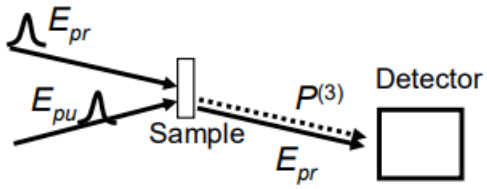

Figure 3.2: Pump-Probe geometry

In a pump-probe experiment, the energy impinging the detector is measured either in presence or not of the pump pulse.
In the case in which the pump pulse is switched off,the incoming energy is given only by the probe electric field. The probe energy that reaches the detector is

$$U_{OFF} = \int_R |E_{probe}(t)|^2 dt$$

In the case in which the pump pulse is switched on, also the nonlinear emitted field will be detected. The probe energy that is collected by the detector is

$$U_{ON} = \int_R |E_{probe}(t) + E^{(3)}(t)|^2 dt$$

We can use an optical modulator (chopper) to modulate the pump pulse.
By calculating the normalized probe energy differences between the cases of pump

switch on and off, we get the differential transmission

$$\frac{\Delta T}{T} = \frac{T^{pump\ on} - T^{pump\ off}}{T^{pump\ off}} \tag{3.2}$$

and for a small nonlinear signal it can be approximated as:

$$\frac{\Delta T}{T}(t,T) \propto \frac{\int_{-\infty}^{\infty} 2Re\{\tilde{E}^*_{probe}(t)\tilde{E}^3(t,T)\}dt}{\int_{-\infty}^{\infty} |E_{probe}(t)|^2 dt} \tag{3.3}$$

We can write the same expression in case of detection with a multichannel detector, which performs a Fourier transform with respect to time t:

$$\frac{\Delta T}{T}(\omega,T) \propto \frac{2Re\{\tilde{E}^*_{probe}(\omega)\tilde{E}^3(\omega,T)\}dt}{\int_{-\infty}^{\infty} |\tilde{E}_{probe}(\omega)|^2 dt} \tag{3.4}$$

In a pump-probe experiment, any detector will be sensitive to the intensity of the probe light, and not to its field.

Because of the excitation driven by the pump pulses, each sample will show different dynamics depending on its electronic level structure, on the pump and probe frequencies and on their relative delay. In the following we explain the main signals that can be distinguished in a pump-probe experiment.
After the pump is transmitted through the sample, the system to transit to the excited state $|1\rangle$. After a delay time of T, the probe pulse impingement the sample and can generate three different transitions, as showing on figure 3.3. The first possibility of transition is the **Photo Absorption (PA)/ Excited-State-Absorption (ESA)** $|1\rangle \rightarrow |2\rangle$. The second possibility is **Stimulated Emission (SE)** $|1\rangle \rightarrow |0\rangle$. Moreover, a **Ground State Bleaching (GSB)/Photobleaching (PB)** signal occur during the process.

In the Ground State Bleaching (GSB), the molecules energy level is initially in the ground state. When the pump pulse is impingement the sample, some molecules will move to the excited state energy level. Afterword, the probe pulse also impingement the sample on the same area but in this time we absorb less transition since some of the molecules have been excited already. Less molecules in the ground state increases the transmission. When we take large delay time T, the population reduce back to the ground state before the probe pulse is arriving. This is a reversible process.
The Stimulated Emission (SE) is a process which the system is transited from the excited state to a lower energy level. The result of the process is a photon amplified.
The Photo-Absorption(PA)/ Excited-State-Absorption (ESA) is an excitation of a system from low energy excited state to a higher energy level.

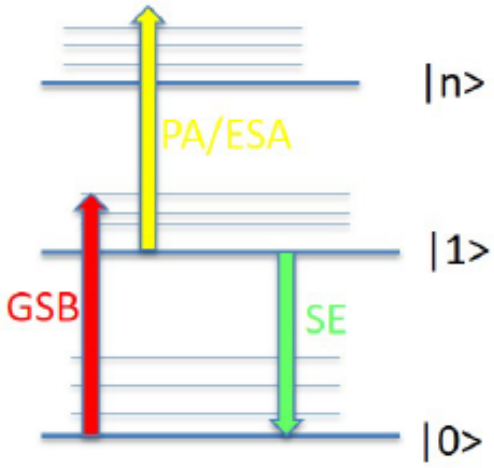

Figure 3.3: Possible signal obtain in Pump-Probe spectroscopy

$\frac{\Delta T}{T}$ will be positive in the case of stimulated emission or GSB. In the case of photo-absorption, the transmission of the probe is reduce and $\frac{\Delta T}{T}$ will be negative

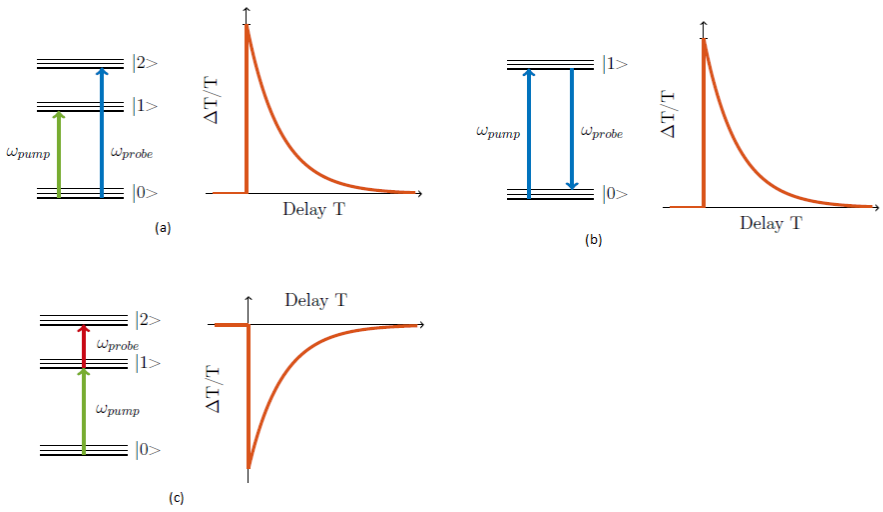

Figure 3.4: (a)Ground State Bleaching (GSB) (b)Stimulated Emission (SE) (c)Excited-State-Absorption (ESA)

3.2 Pump-Probe Set Up

Many setup configurations are possible in order to exploit pump probe spectroscopic technique. The two beams can share the frequency, if they come from the same laser or optical OPA. The signal depends only on the delay between these two pulses. This configuration is called **degenerate pump-probe**. It is not possible to detect pump induced absorption or the creation of new excited state in the molecules with a simple degenerate pump-probe experiment, we need at least two different frequencies for the pump and the probe: this is called Two-colour pump-probe. In order to study all the possible photo absorption signals it is more useful to have a broadband probe to detect absorption of all possible frequencies. Therefore, while the pump pulse is generating at specific wavelength, the probe pulse can be over a wide range of wavelengths by generating it as a white light continuum (see section 2.7). This makes it possible to spectrally resolve pump probe experiment[27].
Figure 3.5 shown a block scheme of a broadband pump probe, starting from a coherent laser source (titanium sapphire, at 1kHz repetition rate). The pump is ultra-short in time in order to obtain a very high resolution. Is generated by a tunable parametric amplification of a certain region of frequency, according to the sample we would investigate. The pump beam needs to be focused onto a sample where it needs to overlap spatially and temporally the probe beam in order to perform pump probe spectroscopy. Moreover the pump is modulated using a mechanical light chopper.

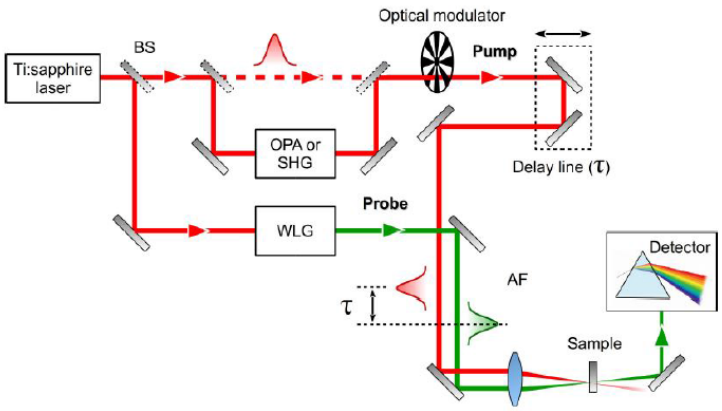

Figure 3.5: Experimental setup configuration of pump probe

After passing through the sample, the probe is spectrally dispersed and then measured in parallel via a (time-integrating) photo-detector array. This gives the transmitted probe spectrum. The spectra are recorded both with the pump on and with the pump blocked. Subtracting these yields the differential transmission

spectrum. Such differential spectra are then recorded as a function of probe delay.

$$\frac{\Delta T}{T}(\omega_{probe}, \Delta t) \tag{3.5}$$

Where T is the transmission and t is the delay time between the pump and the probe.
The resulting time and frequency resolved pump-probe data often provide much richer information than is possible in degenerate measurements (which provide only time resolution).

Chapter 4

Materials and Methods

4.1 Experimental Setup

In this section I am going present the experimental setup that was used to perform pump-probe spectroscopy. As we will see later in the chapter, the required pump spectrum has a wavelength range of the edge of the visible (VIS) range,next to the near ultraviolet (NUV). The requirement of both short time resolution and excitation wavelength in the NUV , made our setup complex.
The experimental setup is shown in figure 4.1. We use Ti:sapphire laser with wavelength of $790nm$, a pulse rate of $2kHz$, pulse duration of around $150fs$ and power of $3W$.
A portion of the laser beam is used for the setup, which is splits into three portions by beam splitters.

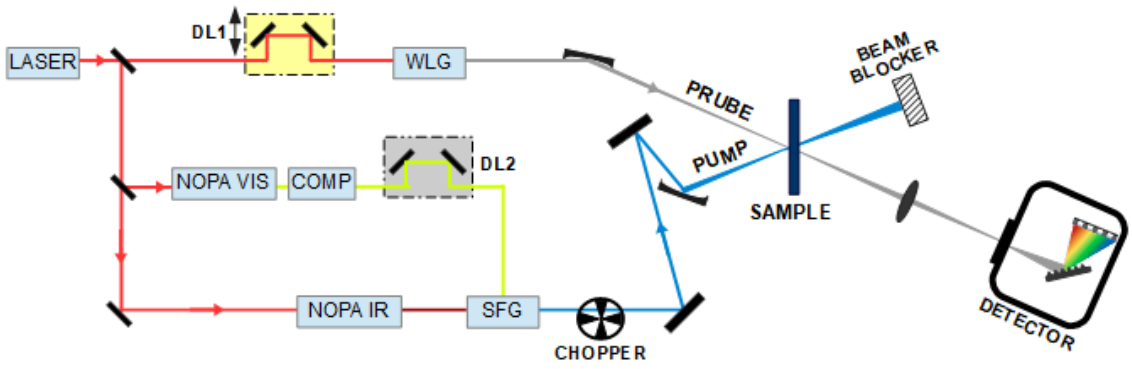

Figure 4.1: Complete experiment setup. LASER: Ti:sapphire, $790nm$, $150fs$, $1kHz$. DL1: adjustable delay line. DL2: fixed delay line. COMP: chirped mirror pulse compressor

In the first portion, the pulse is used to generate white light as explained in

section 2.7. This beam is used as the **probe** pulse in the experiment. In order to control the time delay of the probe pulse with respect to the pump pulse, the beam passes through a motorize delay stage.
The second portion of the laser beam, is used to generate tunable light through a visible NOPA (see section 2.6.2). The output beam of the visible NOPA passes through a pulse compressor (see section 2.8) and afterward it goes to the SFG stage (see section 2.3.1).
The third laser beam portion is continues to the infrared NOPA (see section 2.6.2). The output of the NOPA goes together with the visible NOPA, to the SFG stage in order to generate the pump pulse that needed. In order to have a temporal overlap between the visible beam and the infrared beam, we used a delay line. In figure 4.2 we can see a scheme of the blue light generation, achieved through SFG, using 50 μm thick type I BBO. The output of the SFG setup is used as the **pump** pulse. The energy that is arriving to the ample is around $4nJ$. Figure 4.3 shows that the obtained spectra of the pump beam is between 385 and $450nm$.The duration of the pulse is approximate below $25fs$.

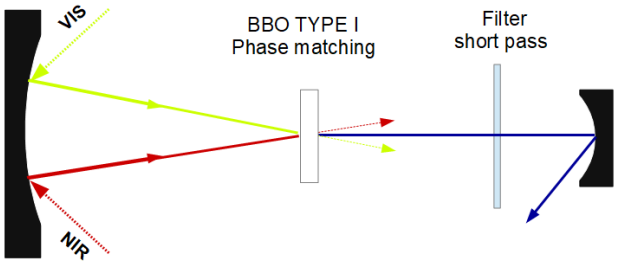

Figure 4.2: Generation of BLUE wavelentgh by SFG

The pump pulse is modulated by a mechanical chopper at a frequency of 1KHZ, in order to obtain a differential transmission signal.
After passing through the sample, the pump beam is blocked whereas the probe pulse continues to the detector. The detector we use is an Optical Multichannel Analyzer (OMA). The OMA contains a grating that disperse different frequency ranges on a linear CCD. The spectrum resolution of the measurement is typically less than 1nm, and it is given by the number of the CCD pixels , the grating type and their distance.

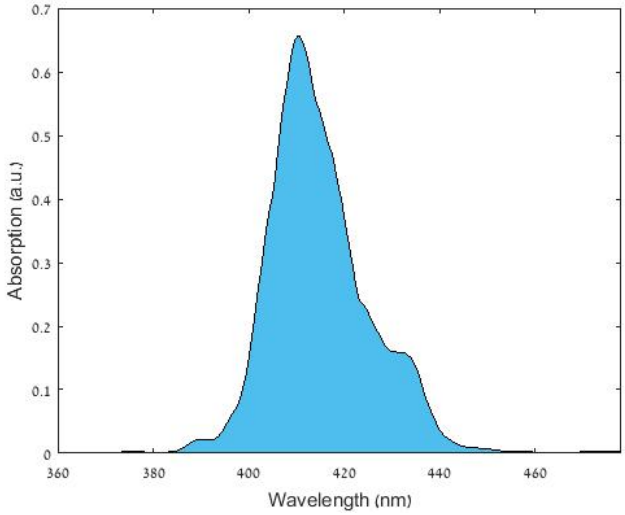

Figure 4.3: Spectrum of the pump beam

4.2 The Samples

4.2.1 Molecular Structure

Most of the sunlight used in photosynthesis is absorbed by light-gathering antenna molecules. The antenna molecules is an array of protein and chlorophyll molecules integrated in the membrane of plants, which transfer light energy to one chlorophyll that has a key role in the photosystem of the plants[1].
Synthetic arrays in which porphyrins are arranged in ring-like structures have been prepared and studied in order to model the natural antennas and reaction centers and for potential use in artificial photosynthesis.
In previous studies, the chromophores are held in large macrocyclic structures via covalent bonds or self-assembly[28]. In others, the porphyrins are organized in wheel-like structures[29]. In all these studies, the interactions between the porphyrins and the other antenna chromophores have not been as strong as those observed in natural photosynthetic antennas.

In this research we used free base porphyrin samples that was synthesized in a new method [1]. The synthesis of the monomer is shown in figure 4.4. The process begins with porphyrin diester 4. Controlled base-catalyzed hydrolysis yields to monoester 5. Coupling 5 to tetrabutylammonium fluoride (TBAF)-assisted esterification by reaction of the acid with a benzyl bromide (Br) smoothly converts the acid to the corresponding ester. The preparation of the dimer and hexamer were similar, but the benzyl bromide was replaced by the appropriate benzyl halide.

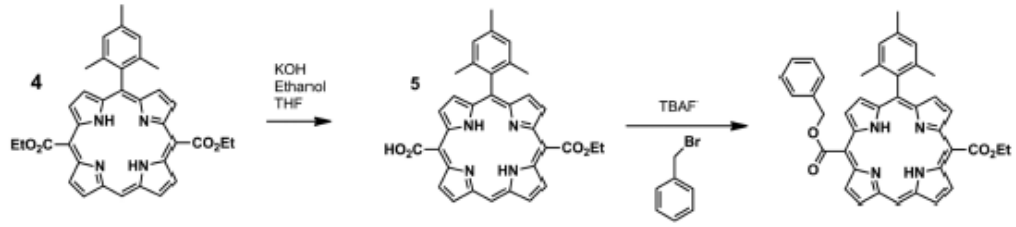

Figure 4.4: Synthetic scheme for preparation of porphyrin monomer. THF = tetrahydrofuran, TBAF = tetra-nbutylammonium fluoride.

In this configuration, the porphyrins has only one meso-aryl substituent (CO_2E_t). Therefore, the acid moiety is available for further functionalization, and because there is no aryl group between it and the porphyrin ring, it allows the construction of arrays in which the porphyrin macrocycles are closer together and therefore can interact more strongly with respect to other porphyrin samples that was studied before.

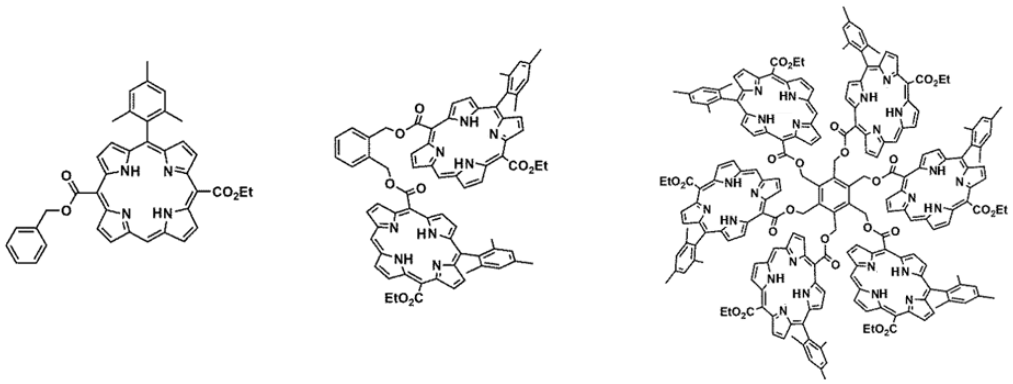

Figure 4.5: Porphyrin molecule. Monomer (right), Dimer (middle), Hexamer (left)

The porphyrins dimers created with the synthetic method are in a twisted stack shape, as can be seen in figure 4.6. This conformation suggests strong $\pi - \pi$ interactions between the macrocycles.
The hexamer indicate formation of three similar twist-stacked dimers, which are arranged in such a way that additional and weaker electronic interactions occur between the pairs of twist-stacked porphyrins (figure 4.7). The twist-stacked dimers configuration is similar to the configuration of bacteriochlorophylls found in some photosynthetic bacteria. Hence, arrays of this type will be good models of the interactions of photosynthetic pigments. They can also be consider as model for in artificial photosynthetic constructs.

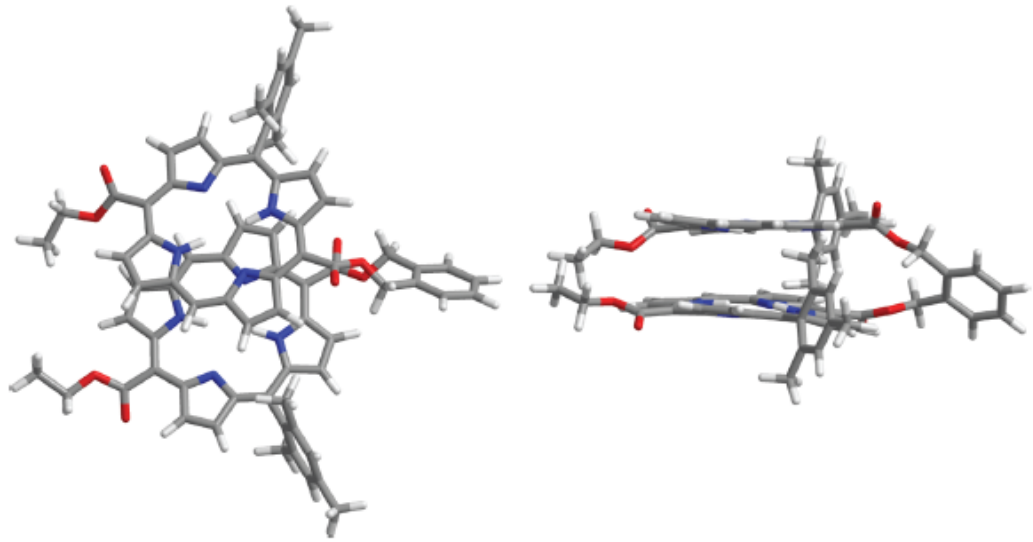

Figure 4.6: Illustration of the porphyrin DIMER sample. **Left:** *Top view* **Right:** *side view.*

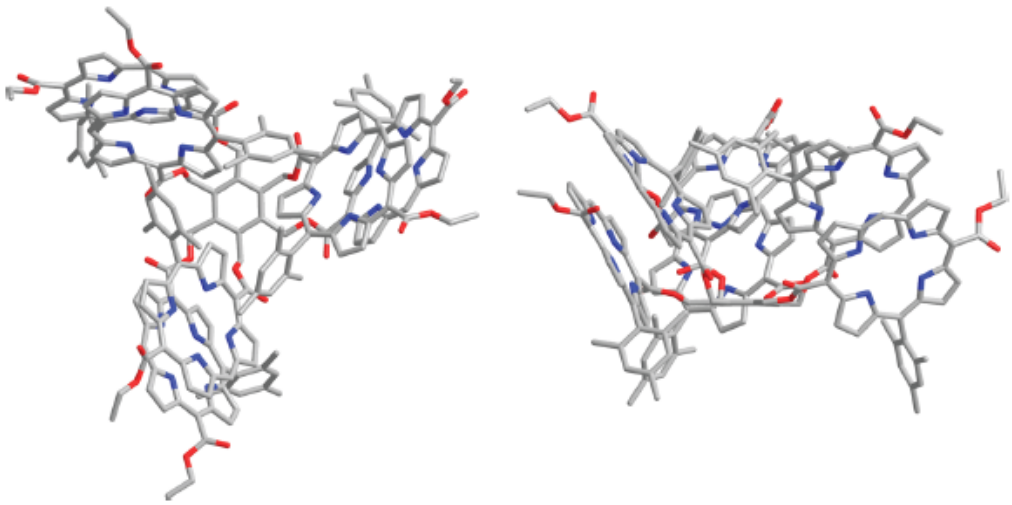

Figure 4.7: Illustration of the porphyrin HEXAMER sample. **Left:** *Top view* **Right:** *side view. The hydrogen atoms are not shown.*

4.2.2 Absorption Spectra

In figure 4.8 we can see the absorption spectrum of the monomer, dimer and hexamer porphyrin in the range from 300 nm to 680 nm. We can see the soret band and the four Q band of the molecules.
The porphyrin monomer shows a soret band peaks at 404 nm and Q band maxima at 503, 539, 581, and 639 nm. These bands are typical for free base porphyrins.

The spectrum of the dimer porphyrin shows a soret band peaks at 402 nm and Q band maxima at 505, 542, 584, and 639 nm.
The haxemer porphyrin, as shown in the figure, has a soret band at 401nm and Q band at 505, 542, 584 and 639 nm.
As can be seen in the figure, the Soret band and the Q band of the dimer and the haxemer are similiar, and they are broadened comparing to the monomer.

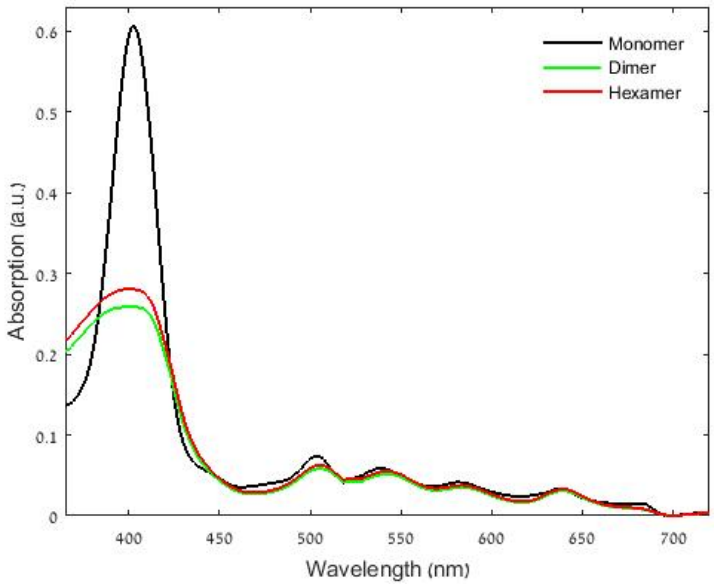

Figure 4.8: Absorption spectrum of monomer, dimer and hexamer of porphyrin

As mentioned above, the experiment setup was built in order to pump the sample in the correct wavelength range in order to excite the sample. We can see in figure 4.9 that we obtained an overlap between the pump pulse and the porphyrins soret band spectrum.

4.3 Global Analysis

Glotaran is a free software program developed at the department of Computational Biophysics of the Vrije Universiteit Amsterdam,for global and target analysis of time-resolved spectroscopy and microscopy data. It is written in R programming language, a software environment for statistical computing. The Glotaran serves as a graphical user interface (GUI) to the R-package TIMP, a package for fitting separable nonlinear models in spectroscopy and microscopy [30][31].

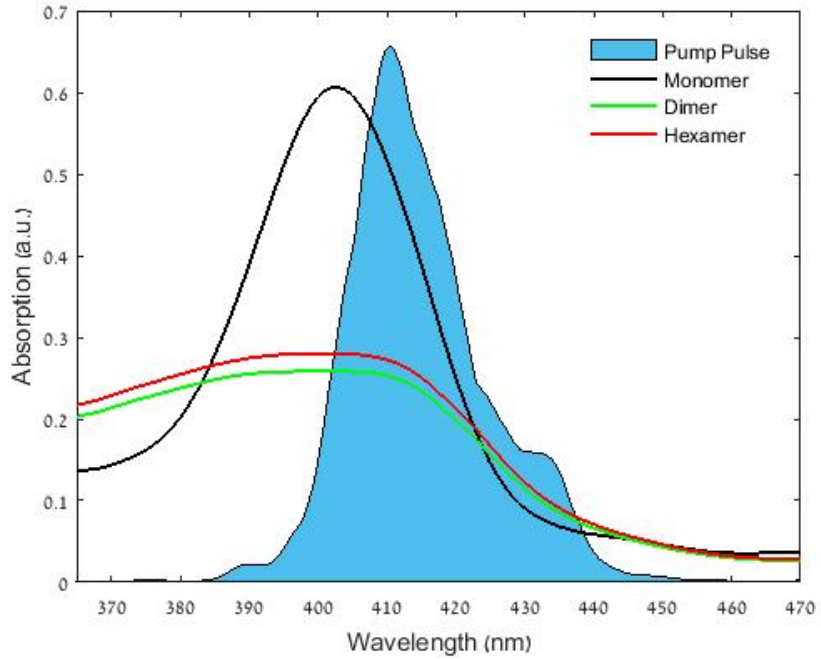

Figure 4.9: Overlap of the pump pulse's spectrum and the porphyrin's absorption for monomer, dimer and hexamer

4.3.1 Theory

The Glotaran modeling is taking into account the noise characteristic and the resolution of the measurements. The Glotaran analysis based on the assumption of noise in data normally distributed with a constant variance. The convolution of the exciting laser shape and the detector response is called the Instrumental Response Function (IRF) and it should be taken into consideration in the modeling process.

The model assumptions are: **Homogeneity** of the system which means that a discrete set of parameters can be used to describe the data; **Separability** which means that the measured time- resolved spectrum Ψ can be represented as a superposition of the contribution of all different components. In another words, when $c_l(t)$ and $\epsilon_l(t)$ are the concentration and the spectrum of the component respectively, the time resolved spectrum can be expressed as

$$\Psi(t, \lambda) = \sum_{l=1}^{n} c_l(t)\epsilon_l(\lambda)$$

The goal is to recover concentration profile c_l as a function of t, and the spectrum profile ϵ_l as a function of λ by a model based description. It can be either a **kinetic model**, or a **spectral model**.
The kinetic model, is a model of the dynamics of the sample. It describes the concentration of components in a measurement over time.Usually, the concentrations are described by linear first order differential equations so the solution is a sum of exponentially decaying function, convoluted with the IRF function.

$$\Psi(t,\lambda) = \sum_{l=1}^{n} e^{(-k_l t)} \circledast IRF(t)\epsilon_l(\lambda)$$

Where k_l is the rate of exponential decay of component l.
Once there is a parametric model-based description of the data, it needs to estimate the parameters. It is obtained by optimizing the vector of parameters that determine the lifetime of each component, while at the same time finding the optimum for the amplitudes of the spectra that together minimize the residuals.

$$min||(\Psi - \sum_{l=1}^{n} c_l(t)\epsilon_l(\lambda))||^2 \tag{4.1}$$

The equation (4.1) can be solved by a technique called variable projection that reduces the separable estimation problem to one [32].
The use of a unified separable nonlinear model to describe all measurements collected over multiple independent variables, and possibly over the course of many experiments, is what is referred to as global analysis. The initial part of the global analysis using kinetic model, is to fit the data with a sufficient number of exponential decays and their amplitudes. The number of the components and their starting value can be estimated based on an educated guess, according to previous studies

In this research we use a sequential kinetic model. The sequential model represent a case where the first energy level gets populated by an input excitation pulse and subsequently forms the second component. The second component decay into a third energy level and so on, until the nth component decays to the ground state. There are two assumption in the sequential model. The first one is ignoring the back-reactions because the energy losses are large enough so the reverse reaction rates is negligible. The second assumption is that there are no losses in the decaying chain to the ground state.

4.3.2 Glotaran User Interface

In the data exploration windows of the Glotaran interface, we can absorve the time resolved spectroscopy data. The data are the differential transmission measured as a function of variable wavelength λ and the variable time delay t. An example of data as it shown in Glotaran interface can be found in figure (4.10).

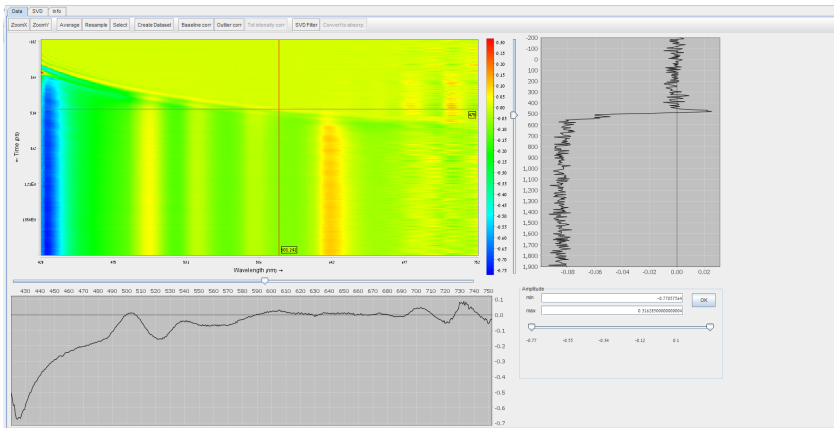

Figure 4.10: Time resolved spectroscopy data. The main figure is the differential transmission measured as a function of wavelength(horizontal axis) and time (vertical axis).The data can be also shown in a specific time trace or spectrum.

The analysis scheme editor (figure 4.11) is the editor for creating and editing the models. It is composed of four sections. The first one is the model specification window, where we define the parameters of the data. The KinPar label represents a number of kinetic rates, the IRFPar represents the IRF function, the Dispersion represents the dispersion of the IRF,the WeightPar can be used to give weights to certain regions of the data and the Cohspec holds the specification for the coherent artifact.
The second section is the datasets specification window. The third section is the output specification window where we choose the maximum number of iterations the model can run. The fourth section is a simulation specification window.

The results of the analysis are shown in figures 4.12 and 4.13. A summary of the estimated parameters of the time constants is shown in a text field. Moreover, we can see the analysis of the result. We will focus in the Evolution Associated Spectra (EAS)(left upper graph in figure 4.13). The EAS is the estimated spectral evolution of each of the individual excited-state species. In the figure, the black curve represent the spectra of the first life time, the red represent the second life time and the blue is the third life time. [33]

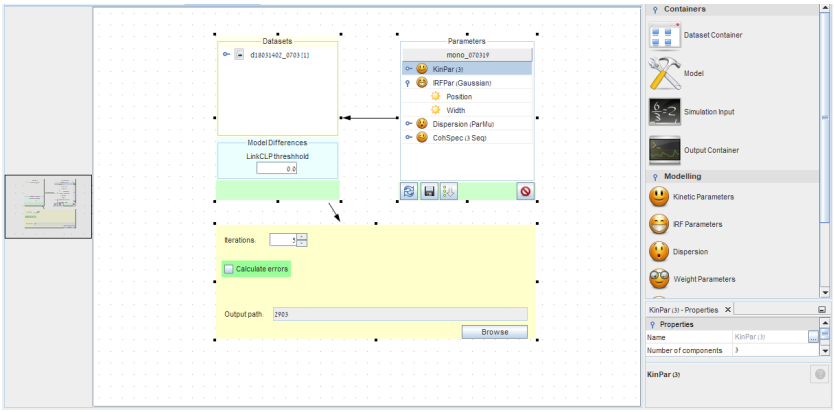

Figure 4.11: Analysis scheme editor

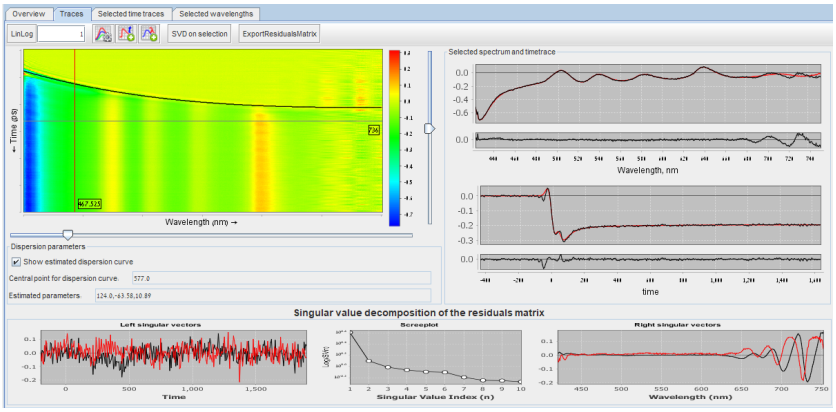

Figure 4.12: Fitting of global analysis of time resolved spectroscopy data

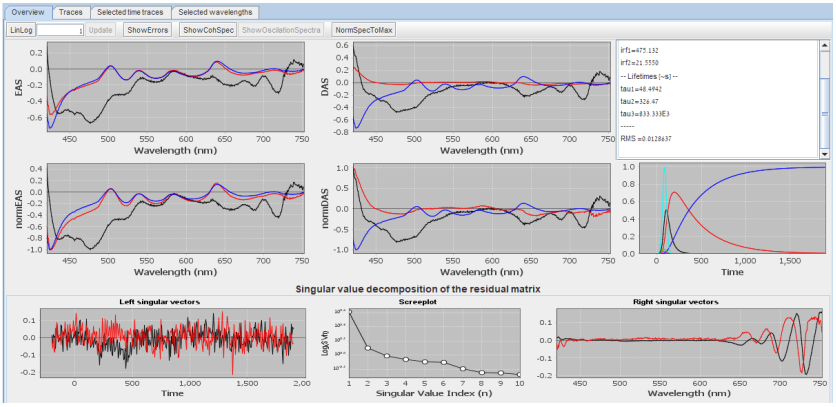

Figure 4.13: Overview of the result of a global analysis of time resolved spectroscopy data

Chapter 5

Experimental Result

In the following chapter I will present the pump probe experiment results of the monomer, dimer and hexamer porphyrin arrays.
Afterward, I will use a global analysis to deepen our understanding of the samples photophysical emission. I will compare the different time constants of each sample array and the different samples.

5.1 Pump Probe on Monomer

The monomer pump-probe map , as shown in figure 5.1, is in the range of white light from 420 nm up to 740 nm, with a time delay goes from negative time to 1340 fs.
The UV pump excites a transition from the ground state S_0 to the excited state S_2. Afterward, we obtain a few different transitions. By choosing a few pump time delays, we can observe the changes in the differential transmission of the monomer porphyrin, as a function of the wavelength spectrum (figure 5.2).
We can see the stimulated emission (SE) that related to the positive peak at 710 nm. Moreover, there are four photo bleaching (PB) transitions, related to the positive peaks at 503 nm, 540 nm, 585 nm and 640 nm.
The photo absorption (PA) is underlying with a peak around 425 nm. We can see a blue shift in this region, according to the transition from S_2 to S_n. The blue shift can be seen in the both figures of the dynamic and spectrum, as shown in figure (5.4 and)

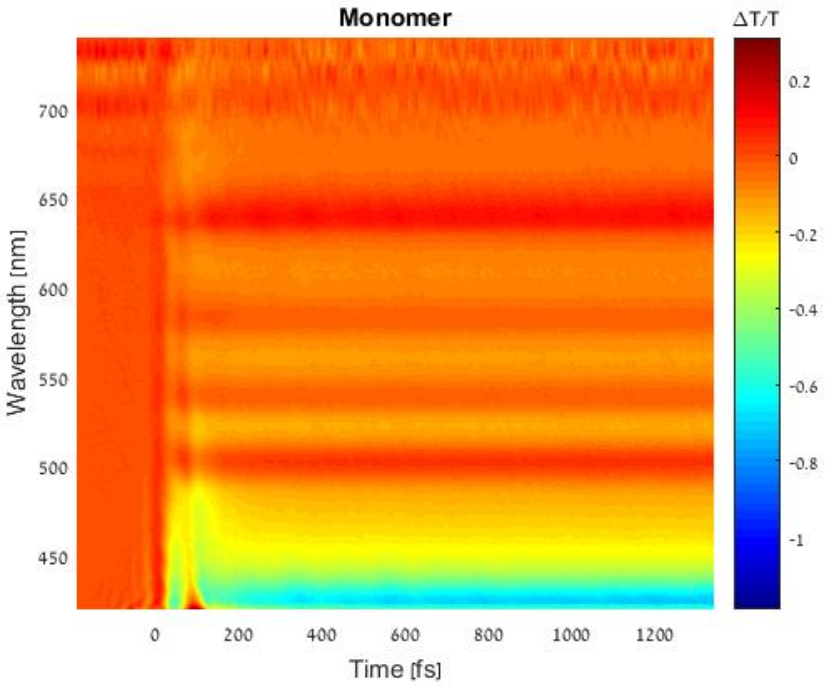

Figure 5.1: 2D Pump-Probe map of porphyrin monomer

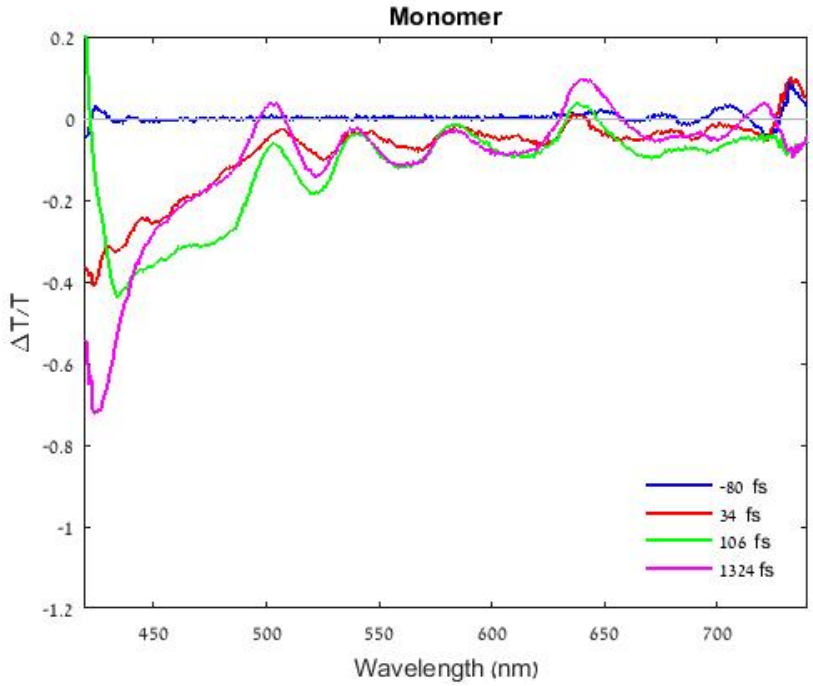

Figure 5.2: Spectra of porphyrin monomer for different time delays

0

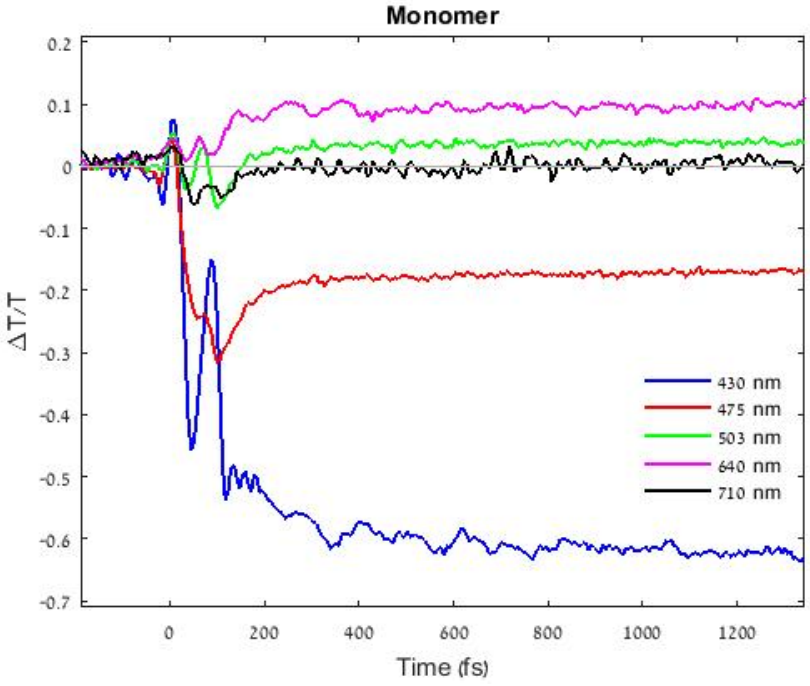

Figure 5.3: Dynamic of porphyrin monomer for different wavelengths

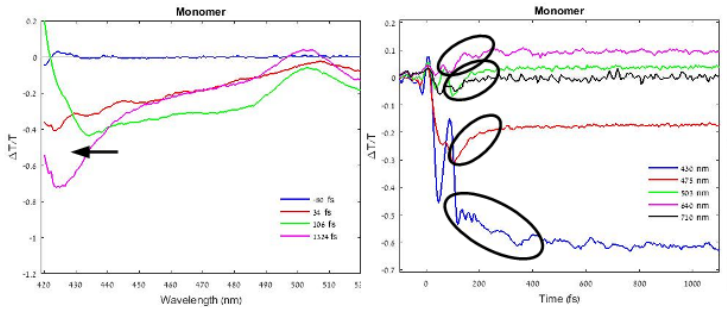

Figure 5.4: Blue shift as a result of the photo absorption (PA) transition from S_2 to S_n. **LEFT:** *Spectrum* **RIGHT:** *Dynamic*

5.2 Pump Probe on Dimer

The 2D pump probe map of the hexamer is shown in figure 5.5. By looking at figures 5.6 and 5.7 we can notice that the behaviour of the dimer is similar to the monomer in the spectra and the dynamic of the pump probe study. The dimer shown SE that related to the positive peak at 710 nm. Moreover, there are PB

transitions, related to the positive peaks at 503 nm, 540 nm, 585 nm and 640 nm and underlying PA with a peak around 425 nm. Moreover,we can see the blue shift similarity to the monomer.
By comparing the spectrum graphs of the two samples we can see that the PA peak of the dimer has a "sharper" shape than the PA peak of the monomer.

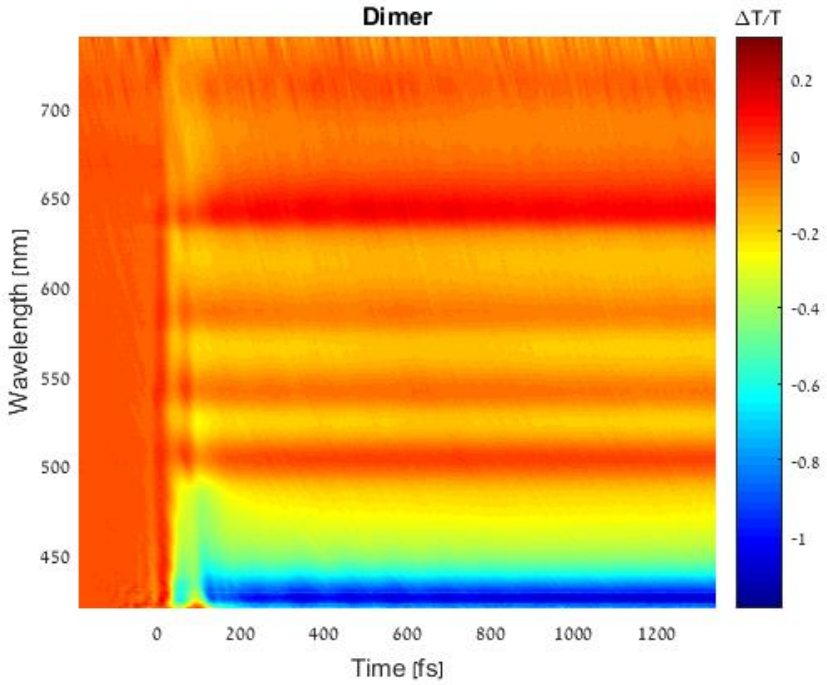

Figure 5.5: 2D Pump-Probe map of porphyrin dimer

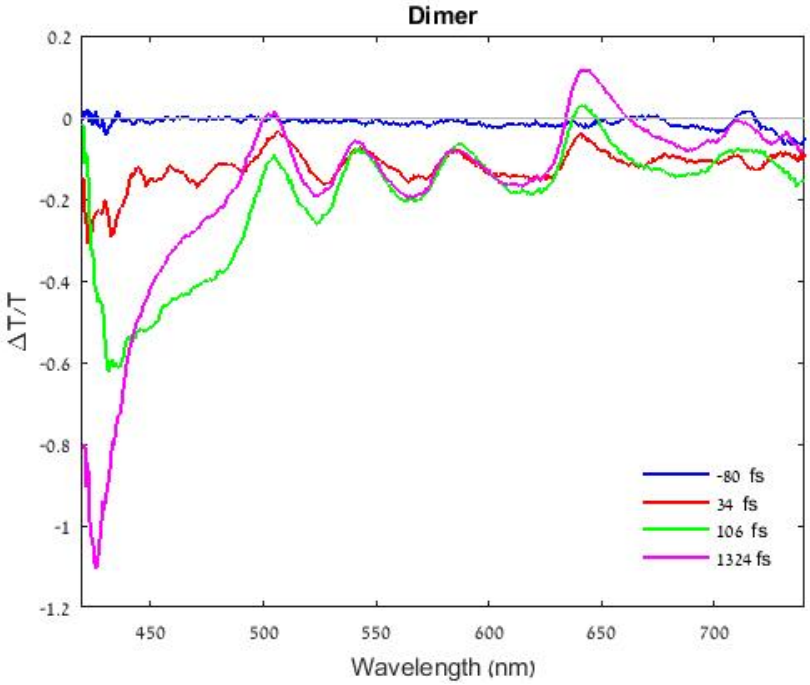

Figure 5.6: Spectra of porphyrin dimer for different time delays

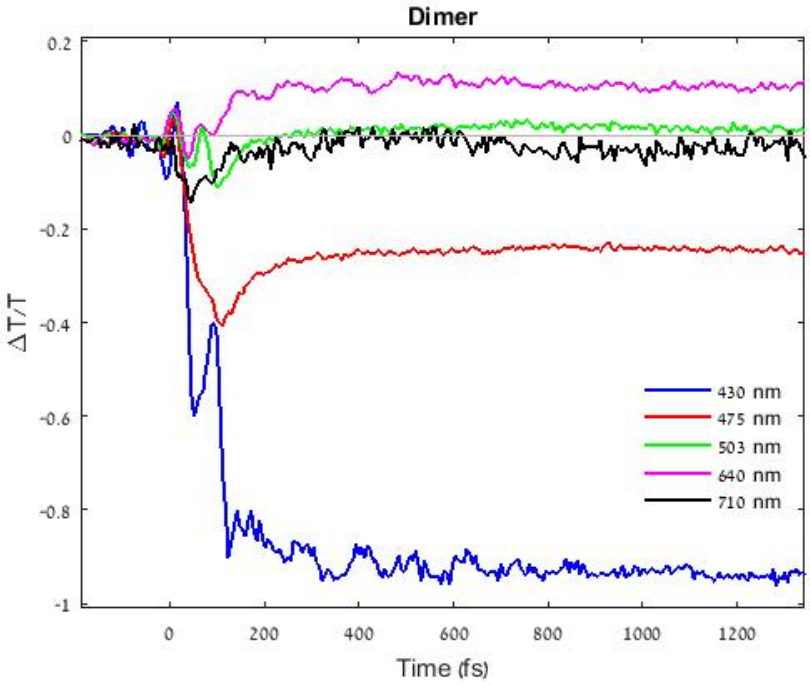

Figure 5.7: Dynamic of porphyrin dimer for different wavelengths

5.3 Pump Probe on Hexamer

The 2D pump probe map of the hexamer is shown in figure 5.8. By looking in figures 5.9 and 5.10 we can observe the transition in the sample. There is a SE transition related to the positive peak at 710 nm, there are four PB transitions, related to the negative peaks at503 nm, 540 nm, 585 nm and 640 nmand a PA with a peak around 425 nm.
As we can see, the hexamer has similar properties like the monomer and the dimer. Though, we can see in the spectrum figure that the peak of the PA transition is more similar to the shape of the dimer PA peak than the one of the monomer. Further, the shape of the hexamer PA peak is "sharper" than the shape of the dimer PA peak.

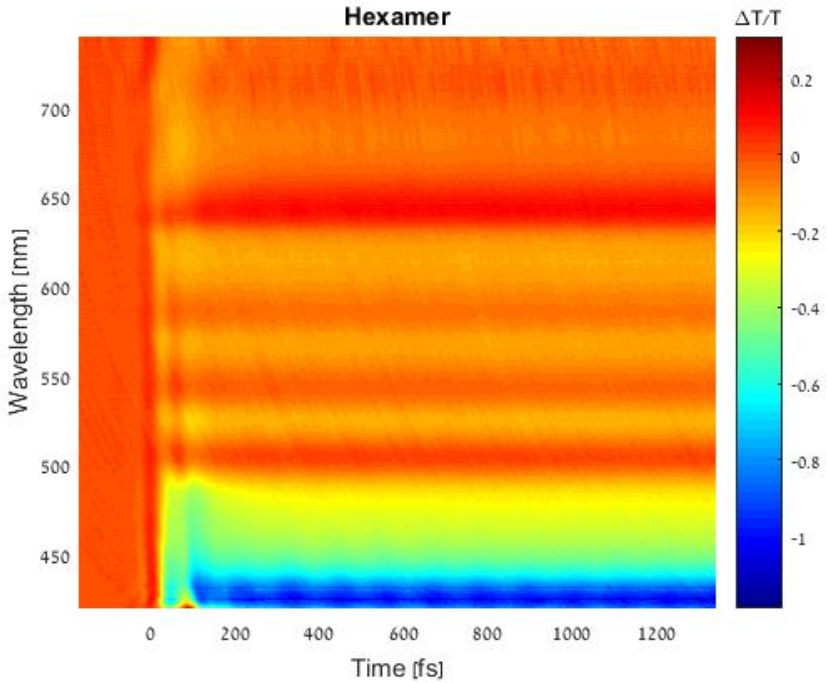

Figure 5.8: 2D Pump-Probe map of porphyrin hexamer

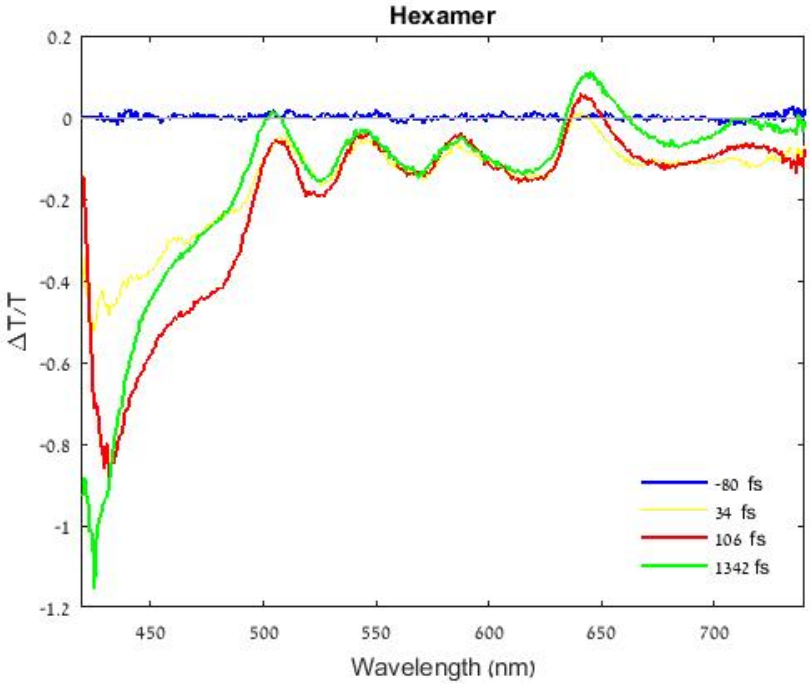

Figure 5.9: Spectra of porphyrin hexamer for different time delays

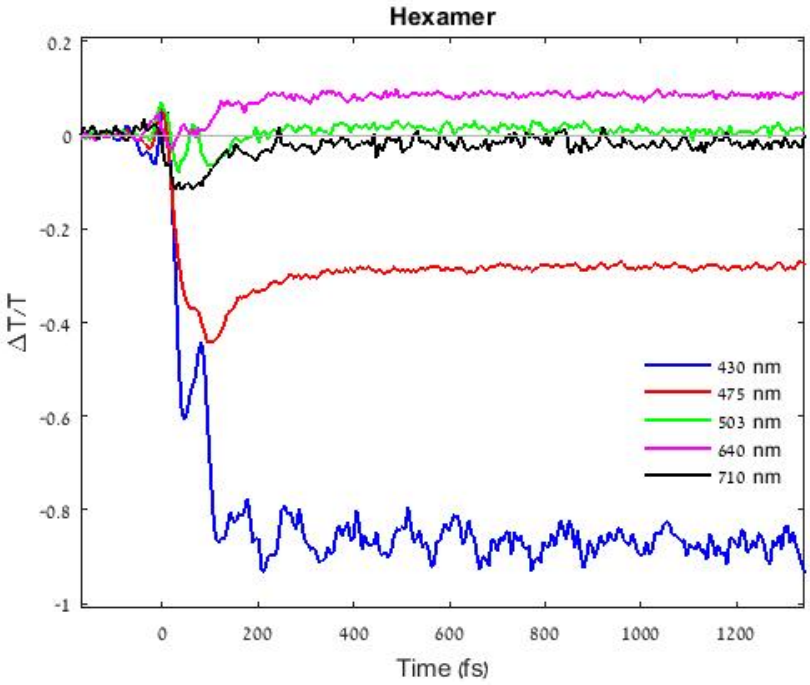

Figure 5.10: Dynamic of porphyrin hexamer for different wavelengths

5.4 Global Analysis

In this section I will present a global analysis for the three samples.
The time constant are shown in figure 5.11. The first time constants τ_1 is fast and related to the Vibrational Relaxation (VIB) within the S_2 band. The second time constant, τ_2, is related to the Internal Conversion (IC) of the molecule, between the S_2 to the S_{1-hot} band. The third time constant τ_3 and the fourth time constant τ_4 are related to internal relaxation processes within S_1. τ_3 is a new time decay, unique for the porphyrin samples we are studying. τ_4 time decay is in the order of the VIB time constant from S_1 hot to cold as was reported in previous studies about porphyrin molecule (see section 1.2). I set τ_4 as a fixed value since there is no influence on the global analysis results for increasing of τ_4 more the 8.33E5 fs, higher value of time decay is out of the time range of the experiment.
We can see that the time decay of each process is fastest in the hexamer and the slowest in the monomer case. Moreover, we can see that the hexamer and the dimer porphyrin arrays are behaving similarity, as we expected according to the similar configuration of the two molecules. In figure 5.12 I presented the time constant of the different samples in Jablonsky diagram.

TIME CONSTANTS [femtosecond]				
	Monomer	Dimer	Hexamer	
Tau1	48	35	27	VIB within S_2
Tau2	326	103	93	IC S_2 to S_{1-hot}
Tau3		975	4697	S_1 Relaxation
Tau4	8.33E5 *	8.33E5 *	8.33E5 *	VIB within S_1

*Figure 5.11: Time constants of monomer, dimer and hexamer porphyrin as obtained by Glotaran. *****: Fixed values, see text*

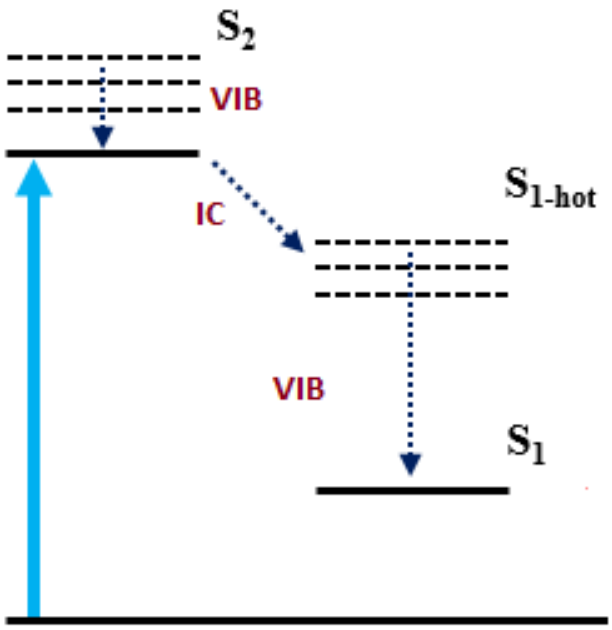

Figure 5.12: Jablonsky diagram of the porphyrin. VIB- vibrational relaxation. IC- Internal Conversion

Once we found the time constants of the samples, we can look at the Evolution Associated Spectra (EAS). The EAS is the estimated spectra in the time decay components , and presented in figures 5.14, 5.13 and 5.15 for the monomer, dimer and hexamer respectively. Thee black curve is the spectra of τ_1, the red curve is the second life time τ_1. The green curve is the third time constant τ_3 of the hexamer and dimer, and the blue is the last time constant.

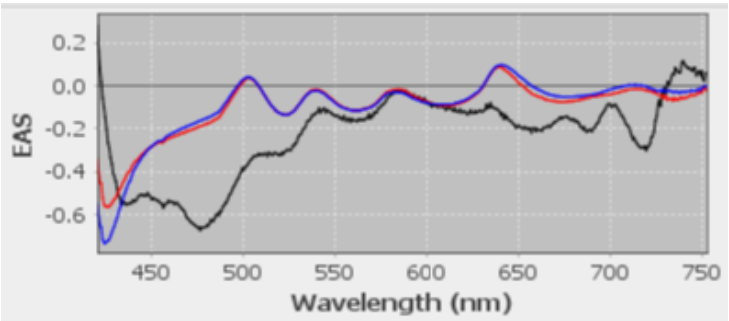

Figure 5.13: Evolution Associated Spectra (EAS) of porphyrin mono (By Glotaran)

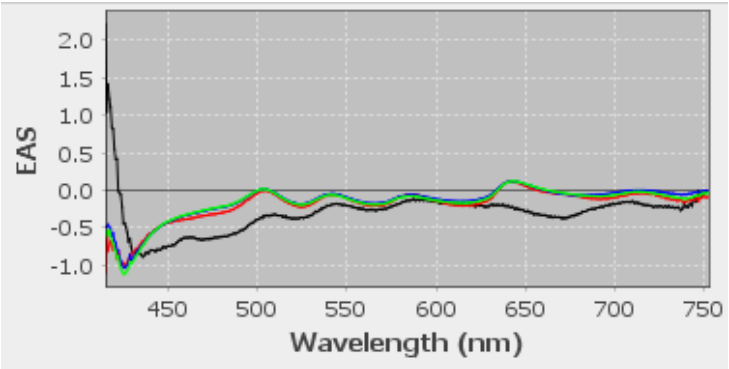

Figure 5.14: Evolution Associated Spectra (EAS) of porphyrin dimer (By Glotaran)

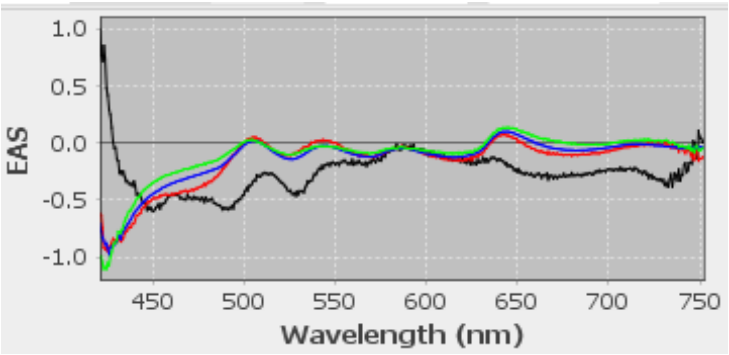

Figure 5.15: Evolution Associated Spectra (EAS) of porphyrin hexamer(By Glotaran)

It is helpful to compare the individual wavelength's dynamic to the dynamic we obtained in the global analysis. The mathematical function of the dynamic is proportional to $\sum_i A_i exp(-(t-t_0)/\tau_i) * He(t-t_0)$ where t_0 is the signal starting time, τ is the time decay constant and it indicates the time constants involved in the transition process. As shown in figure 5.16, the time constants of the monomer, as obtained from the individual wavelength fitting are $\tau_1 = 66fs$, $\tau_2 = 323fs$. In the case of the dimer and the hexamer, as shown in figures 5.17 and 5.18 respectively, three exponents equations fitting was done. The result of the dimer time constants is $\tau_1 = 64fs$, $\tau_2 = 94fs$, $\tau_3 = 3915fs$ whereas the result of the hexamer time constants is $\tau_1 = 60fs$, $\tau_2 = 89fs$, $\tau_3 = 3704fs$
By comparing the result of the individual fitting and the result of the Glotaran analysis, we can see that the main results are consistent. We can see that the VIB time decay τ_1 is similar for the monomer, dimer and hexamer samples. Moreover, the IC time decay, τ_2 of the dimer and hexamer are similar to each other and shorter than the monomer. The third time constant, τ_3, is different from the value we obtained in the Glotaran. Since global analysis method is modeling the

transitions in the sample by using all the experiment data, I will consider the Glotaran result value of τ_3 as more accurate.

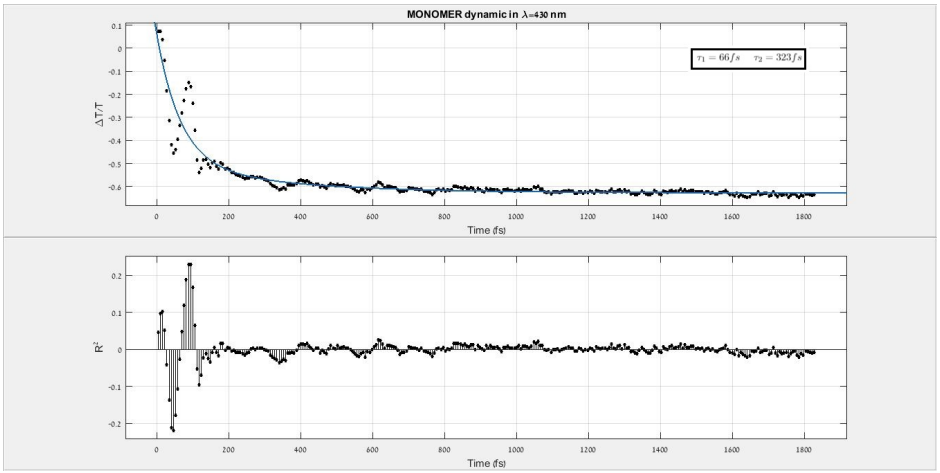

Figure 5.16: Dynamic of porphyrin MONOMER at $\lambda = 430nm$. **TOP:** *Black dots- data of the experiment. Blue curve- fitting* **BOTTOM:** *Residual of the fitting*

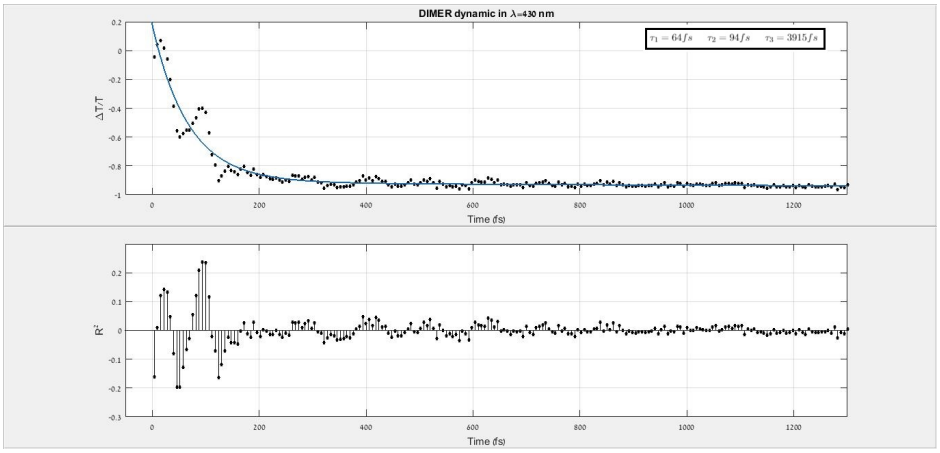

Figure 5.17: Dynamic of porphyrin DIMER at $\lambda = 430nm$. $\tau_1 = 66fs$, $\tau_2 = 323fs$.$\tau_1 = 64fs$, $\tau_2 = 94fs$, $\tau_3 = 3915fs$. **TOP:** *Black dots- data of the experiment. Blue curve- fitting* **BOTTOM:** *Residual of the fitting*

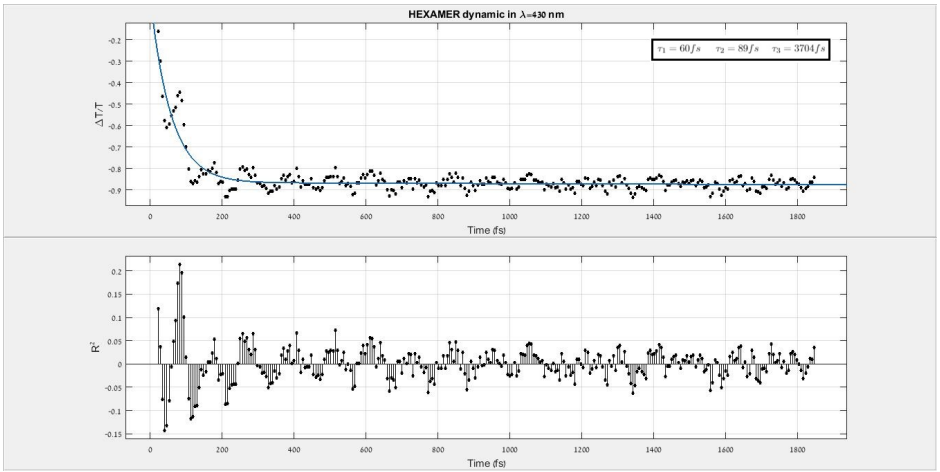

Figure 5.18: Dynamic of porphyrin HEXAMER at $\lambda = 430nm$. $\tau_1 = 60fs$, $\tau_2 = 89fs$, $\tau_3 = 3704fs$. **TOP:** *Black dots- data of the experiment. Blue curve- fitting* **BOTTOM:** *Residual of the fitting*

Chapter 6

Conclusion

In this thesis I developed and characterized a pump-probe spectroscopy setup in the edge of the visible range, in the aim of studying the structural configuration of free base porphyrin and analyzing ultra fast processes in which the porphyrin is involved.
The free base porphyrin sample was synthesized in an innovative method that mimics the natural configuration of porphyrin in photosynthetic bacteria in nature. Photosynthesis is natures way to harness the energy of the sun and convert it efficiently into chemical energy. If engineers would like to create artificial photosynthesis they must first understand the delicate dynamics of porphyrin.

In order to generate a pump pulse in the range of the visible spectrum edge, we used two NOPA. The first NOPA is in the visible spectrum and the other in the infrared spectrum. Both NOPA's outputs arrived together to the SFG stage and generated the pump pulse. The pump pulse is in the range between 385 and 450 nm with energy around 4nJ and duration below 25 fs. The probe pulse was created by a white light generation stage and it is in the range between 385 and 450 nm.

Thanks to the high time resolution setup, we were able to obtain important information about the dynamics of the monomer, dimer and hexamer free base porphyrin. We have found the time constants of the free base porphyrin for the monomer, dimer and hexamer configuration. By knowing the time constants, we can compare the three samples.
I discovered the time constants of each sample by global analysis of the pump probe experiment data. The results demonstrated that the vibration relaxation (VIB) within the S_2 energy level is longest for the monomer sample and shortest for the hexamer sample, while the dimer time decay is in the middle. The inter-

nal conversion (IC) between the S_2 to the S_{1-hot} is the longest in the monomer sample, but in contrast to the VIB, the dimer and the hexamer time constants are very similar to each other, and far from the monomer. This result is indicates the similar configurations of the dimer and the hexamer.

Bibliography

[1] Y. Terazono, G. Kodis, M. Chachisvilis, B. R. Cherry, M. Fournier, A. Moore, T. A. Moore, and D. Gust, "Multiporphyrin arrays with π - π interchromophore interactions", *Journal of the American Chemical Society*, vol. 137, pp. 245–258, 1 Dec. 2014. DOI: 10.1021/ja510267c.

[2] F. E. Dayan and E. A. Dayan, "Porphyrins: One ring in the colors of life: A class of pigment molecules binds king george iii, vampires and herbicides", *American Scientist*, vol. 99, pp. 236–243, Jun. 2011. DOI: 10.1511/2011.90.236.

[3] T. P. Wijesekera and D. Dolphin, "Some preparations and properties of porphyrins", *Advances in Experimental Medicine and Biology*, vol. 193, pp. 229–266, 1985. DOI: https://doi.org/10.1007/978-1-4613-2165-1.

[4] L.-G. Lechoslaw, "Porphyrin chemistry research group", *University of Wroclaw, Wroclaw, Poland*, Mar. 2019. [Online]. Available: http://llg.chem.uni.wroc.pl/?Molecules%3BPorphyrins___Porphyrin_Primer___Basics.

[5] R. Giovannetti, "The use of spectrophotometry uv-vis for the study of porphyrins", *Macro To Nano Spectroscopy*, pp. 87–108, Jun. 2012. DOI: 10.5772/2503.

[6] G. Martin, "Spectra of porphyrins", *Journal of Molecular Spectroscopy*, vol. 6, pp. 138–163, 1961.

[7] R. V. Maximiano, E. Piovesan, S. C. Zilio, A. E. H. Machado, R. d. Paula, J. A. S. Cavaleiro, I. E. Borissevitch, A. S. Ito, P. J. Goncalves, and N. M. Barbosa Neto, "Excited-state absorption investigation of a cationic porphyrin derivative", *Journal of Photochemistry and Photobiology A: Chemistry*, vol. 214, pp. 115–120, 2-3 Aug. 2010. DOI: 10.1016/j.jphotochem.2010.06.007.

[8] D. Dolphin, *The Porphyrins Volume III*. Elsevier, December 1978.

[9] "Jablonski diagram", *LibreTexts Library*, Jul. 2016. [Online]. Available: https://chem.libretexts.org/.

[10] J. S. Baskin, H.-Z. Yu, and A. H. Zewail, "Ultrafast dynamics of porphyrins in the condensed phase: I. free base tetraphenylporphyrin", *The Journal of Physical Chemistry A*, vol. 106, pp. 9837–9844, Aug. 2002. DOI: 10.1021/jp020398g.

[11] H. S. Cho, H. Rhee, J. K. Song, C.-K. Min, M. Takase, N. Aratani, S. Cho, A. Osuka, T. Joo, and D. Kim, "Excitation energy transport processes of porphyrin monomer, dimer, cyclic trimer, and hexamer probed by ultrafast fluorescence anisotropy decay", *Journal of American Chemical Society*, vol. 125, pp. 5849–5860, Apr. 2003. DOI: 10.1021/ja021476g.

[12] M. Kullmann, A. Hipke, P. Nuernberger, T. Bruhn, D. C. G. Gotz, M. Sekita, D. M. Guldi, G. Bringmannb, and T. Brixner, "Ultrafast exciton dynamics after soret- or q-band excitation of a directly β,β'-linked bisporphyrin", *Fhysical Chemistry Chemical Physics*, vol. 14, pp. 8038–8050, Apr. 2012. DOI: 0.1039/c2cp23608g.

[13] B. Abraham, J. Nieto-Pescador, and L. Gundlach, "Ultrafast relaxation dynamics of photoexcited zinc-porphyrin: Electronic-vibrational coupling", *Physical Chemistry Letters*, vol. 7, pp. 3151–3156, Aug. 2016. DOI: 10.1021/acs.jpclett.6b01439.

[14] Y. Venkatesh, M. Venkatesan, B. Ramakrishna, and P. R. Bangal, "Ultrafast time-resolved emission and absorption spectra of meso-pyridyl porphyrins upon soret band excitation studied by fluorescence up-conversion and transient absorption spectroscopy", *Physical Chemistry*, vol. 120, pp. 9410–9421, 2016. DOI: 10.1021/acs.jpcb.6b05767.

[15] P. C. Mandal, M. Goto, and M. Sasaki, "Removal of nickel and vanadium from heavy oils using supercritical water", *Journal of the Japan Petroleum Institute*, vol. 57, pp. 18–28, Jan. 2014. DOI: 10.1627/jpi.57.18. [Online]. Available: https://www.researchgate.net/publication/271352587_Removal_of_Nickel_and_Vanadium_from_Heavy_Oils_Using_Supercritical_Water.

[16] S. V. Bhat, B. A. Nagasampagi, and M. Sivakumar, *Chemistry of Natural Products*. Springer, 1899.

[17] X. HUANG, K. NAKANISHI, and N. BEROVA, "Porphyrins and metalloporphyrins: Versatile circular dichroic reporter groups for structural studies", *Chirality*, vol. 12, pp. 237–255, 4 Apr. 2000. DOI: 12:237255(2000).

[18] F. Siebert and P. Hildebrandt, *Vibrational Spectroscopy in Life Science*. John Wiley & Sons, Inc, 2008.

[19] I. B. Bersuker, *Electronic Structure and Properties of Transition Metal Compounds: Introduction to the Theory, Second Edition*. John Wiley & Sons, Inc, 2010.

[20] *Diffraction Grating Spectrometer: Design and Collected Spectra*. Theremino System.

[21] G. Cerullo, *Photonics II: Physics of Ultrafast Processes*. lecture notes, Politecnico di Milano, September-December 2017.

[22] A. M. Weiner, *Ultrafast Optics*. John Wiley & Sons, Inc, 2009.

[23] C Manzoni and G Cerullo, "Design criteria for ultrafast optical parametric amplifiers", *Jornal of Optics*, vol. 18, Aug. 2016. DOI: 10.1088/2040-8978/18/10/103501.

[24] G. Cerullo and S. De Silvestri, "Ultrafast optical parametric amplifiers", *Review of Scientific Instruments*, vol. 74, 1 Jan. 2003. DOI: 10.1063/1.1523642.

[25] G. Cerullo, D. N. De Silvestri Sandro Fittinghoff, J. A. Squier, C. P. J. Barty, J. N. Sweetser, R. Trebino, and M. Muller, "Collinear type *ii* second-harmonic-generation frequency-resolved optical gating for use with high-numerical-aperture objectives", *Optics Letters*, vol. 23, pp. 1046–1048, 13 Jul. 1998.

[26] S. Mukamel, *Principles of Nonlinear Optical Spectroscopy*. Oxford University Press, 1995.

[27] R. Borrego Varillas, A. Candeo, D. Viola, M. Garavelli, S. De Silvestri, G. Cerullo, and C. Manzoni, "Microjoule-level, tunable sub-10 fs uv pulses by broadband sum-frequency generation", *Optics Letters*, vol. 39, pp. 3849–3852, 13 Jul. 2014. DOI: 10.1364/OL.39.003849.

[28] M. C. O'Sullivan, J. K. Sprafke, D. V. Kondratuk, C. Rinfray, T. D. W. Claridge, A. Saywell, M. O. Blunt, J. N. O'Shea, P. H. Beton, M. Malfois, and H. L. Anderson, "Vernier templating and synthesis of a 12-porphyrin nanoring", *Nature*, vol. 469, pp. 72–75, Jan. 2011. DOI: 10.1038/nature09683.

[29] E. Hao, F. R. Fronczek, and M. G. H. Vicente, "Synthesis of oxaclixarene-locked bisporphyrons and higher oligomers", *The Journal of Organic Chemistry*, vol. 71, pp. 1233–1236, Sep. 2005. DOI: 10.1021/jo051964h.

[30] J. J. Snellenburg, *Glotaran: a tool for interactive global and target analysis of time-resolved spectroscopy and microscopy data.* (Unpublished master's thesis).VU University Amsterdam,Amsterdam,The Netherlands.

[31] H. M. van Stokkum, *Global and target analysis of time-resolved spectra.* "lecture notes, VU University Amsterdam", 2016.

[32] G. Golub and V Pereyra, "The differentiation of pseudo-inverses and nonlinear least squares problems whose variables separate", *SIAM Journal on Numerical Analysis*, vol. 10, pp. 413–432, Apr. 1973. DOI: 10.1137/0710036.

[33] C. Hippius, I. H. M. van Stokkum, E. Zangrando, W. R. M., and F. Wurthner, "Excited state interactions in calix[4]arene-perylene bisimide dye conjugates: Global and target analysis of supramolecular building blocks", *The Journal of Physical Chemistry*, vol. 111, pp. 13 988–13 996, 37 Aug. 2007. DOI: 10.1021/jp0733825.